The vSNAREs VAMP2 and VAMP4 control recycling and intracellular sorting of post-synaptic receptors in neuronal dendrites

May Bakr, Damien Jullié, Julia Krapivkina, Vincent Paget-Blanc, Lou Bouit, Jennifer Petersen, Natacha Retailleau, Christelle Breillat, Etienne Herzog, Daniel Choquet, et al.

Cell Reports

Article

The vSNAREs VAMP2 and VAMP4 control recycling and intracellular sorting of post-synaptic receptors in neuronal dendrites

Graphical abstract

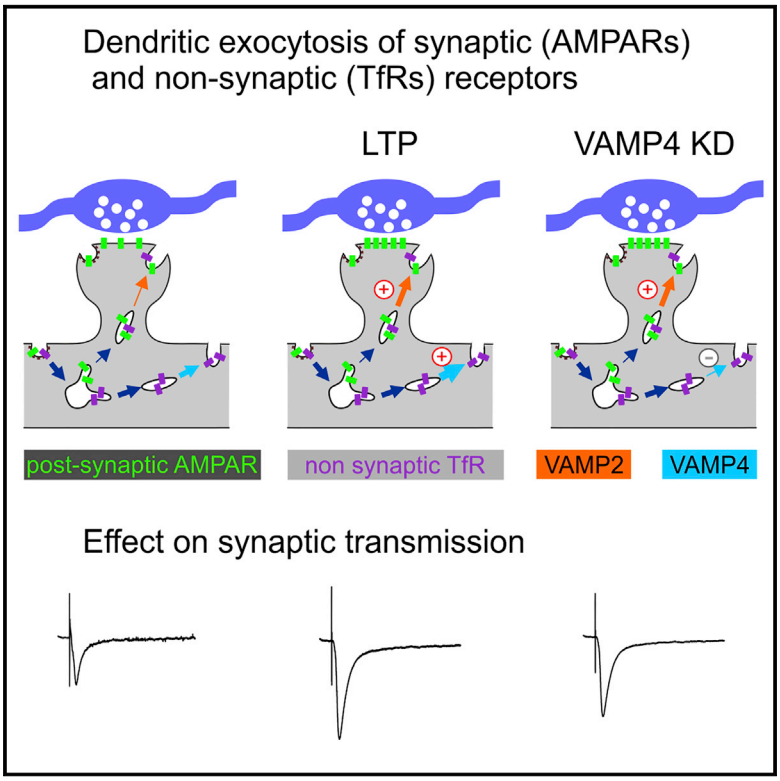

Authors

May Bakr, Damien Jullié, Julia Krapivkina, ..., Etienne Herzog, Daniel Choquet, David Perrais

Correspondence

david.perrais@u-bordeaux.fr

In brief

Post-synaptic exocytosis plays a major role in regulating synaptic transmission and plasticity. Bakr et al. identify two vesicular SNARE proteins, VAMP2 and VAMP4, necessary for exocytosis of recycling endosomes (REs). In particular, VAMP4 is necessary for RE exocytosis and the sorting of AMPA receptors to a specialized RE-derived compartment.

Highlights

- VAMP2 and 4 mediate the exocytosis of somato-dendritic recycling endosomes (REs)
- VAMP2 mediates the exocytosis of a small subset of RE-containing AMPARs
- VAMP4 depletion accelerates GluA1 recycling and increases post-synaptic currents
- Increased basal synaptic transmission partially occludes LTP expression

Bakr et al., 2021, Cell Reports *36*, 109678
September 7, 2021
https://doi.org/10.1016/j.celrep.2021.109678

CellPress

Cell Reports

CellPress
OPEN ACCESS

Article

The vSNAREs VAMP2 and VAMP4 control recycling and intracellular sorting of post-synaptic receptors in neuronal dendrites

May Bakr,[1] Damien Jullié,[1,3] Julia Krapivkina,[1] Vincent Paget-Blanc,[1] Lou Bouit,[1] Jennifer D. Petersen,[1,4] Natacha Retailleau,[1] Christelle Breillat,[1] Etienne Herzog,[1] Daniel Choquet,[1,2] and David Perrais[1,5,*]

[1]Univ. Bordeaux, CNRS, Interdisciplinary Institute for Neuroscience, IINS, UMR 5297, 33000 Bordeaux, France
[2]Univ. Bordeaux, CNRS, INSERM, Bordeaux Imaging Center, BIC, UMS 3420, US 4, 33000 Bordeaux, France
[3]Present address: University of California, San Francisco, San Francisco, CA, USA
[4]Present address: National Institute of Child Health and Human Development, National Institutes of Health, Bethesda, MD 20892, USA
[5]Lead contact
*Correspondence: david.perrais@u-bordeaux.fr
https://doi.org/10.1016/j.celrep.2021.109678

SUMMARY

The endosomal recycling system dynamically tunes synaptic strength, which underlies synaptic plasticity. Exocytosis is involved in the expression of long-term potentiation (LTP), as postsynaptic cleavage of the SNARE (soluble NSF-attachment protein receptor) protein VAMP2 by tetanus toxin blocks LTP. Moreover, induction of LTP increases the exocytosis of transferrin receptors (TfRs) and markers of recycling endosomes (REs), as well as post-synaptic AMPA type receptors (AMPARs). However, the interplay between AMPAR and TfR exocytosis remains unclear. Here, we identify VAMP4 as the vesicular SNARE that mediates most dendritic RE exocytosis. In contrast, VAMP2 plays a minor role in RE exocytosis. LTP induction increases the exocytosis of both VAMP2- and VAMP4-labeled organelles. Knock down (KD) of VAMP4 decreases TfR recycling but increases AMPAR recycling. Moreover, VAMP4 KD increases AMPAR-mediated synaptic transmission, which consequently occludes LTP expression. The opposing changes in AMPAR and TfR recycling upon VAMP4 KD reveal their sorting into separate endosomal populations.

INTRODUCTION

The endosomal system in neuronal dendrites is essential for the maintenance of neuronal polarity, synaptic transmission, and the expression of synaptic plasticity, as well as other forms of signaling (Bentley and Banker, 2016; Kennedy and Ehlers, 2011). In many forms of synaptic plasticity, such as long-term potentiation (LTP) of excitatory synapses in CA1 hippocampal pyramidal neurons, the increase in synapse strength is mediated by the addition of post-synaptic glutamate AMPA-type receptors (AMPARs), which mediate excitatory post-synaptic currents (EPSCs) (Granger and Nicoll, 2013; Huganir and Nicoll, 2013). Consistent with the role for AMPAR exocytosis in LTP, a specific block of vesicle fusion in the post-synaptic neuron by dialysis of botulinum toxin B (BoNT-B) or tetanus toxin (TeNT), which cleave the SNARE (soluble NSF-attachment protein receptor) proteins VAMP1–VAMP3, abolishes LTP in acute slices (Lledo et al., 1998), cultured organotypic slices (Penn et al., 2017), or dissociated cultures (Lu et al., 2001). In addition, dialysis of TeNT or BoNT-B induces a marked decrease of EPSC amplitude in 10 to 20 min (Lüscher et al., 1999; Penn et al., 2017; Wang et al., 2007). This suggests that exocytosis is required not only for synaptic plasticity but also for the maintenance of synaptic transmission at all times. By contrast, acutely blocking receptor internalization by blocking endocytosis mediated by dynamin leads to the increase of EPSC amplitude, also within 10 to 20 min (Glebov et al., 2015; Lüscher et al., 1999; Wang et al., 2007). These results led to the model in which AMPARs are constitutively internalized and recycled (Ehlers, 2000; Passafaro et al., 2001), and modulation of these processes mediate, at least in part, synaptic plasticity.

Effectively, recycling endosomes (REs), which contain internalized receptors, have been identified as the intracellular organelles necessary for the expression of LTP. Overexpression of a dominant-negative mutant of Rab11a, a marker of REs and major regulator of RE function (Welz et al., 2014), blocks LTP (Brown et al., 2007; Park et al., 2004). Moreover, live cell imaging of cultured neurons has shown that the transferrin receptor (TfR), a classical marker of REs, fused to GFP, was transported into dendritic spines after the induction of chemical LTP (cLTP) (Park et al., 2006) through the calcium-dependent binding of myosin V (Correia et al., 2008; Wang et al., 2008). Finally, TfR exocytosis, detected with TfR fused to the pH sensitive variant of GFP superecliptic pHluorin (SEP), is increased after cLTP induction (Hiester et al., 2017; Keith et al., 2012; Kennedy et al., 2010), and recycling of the internalized ligand Tf is similarly increased (Park et al., 2004). Likewise, the exocytosis of AMPAR subunits GluA1–GluA3 labeled with SEP is increased after the

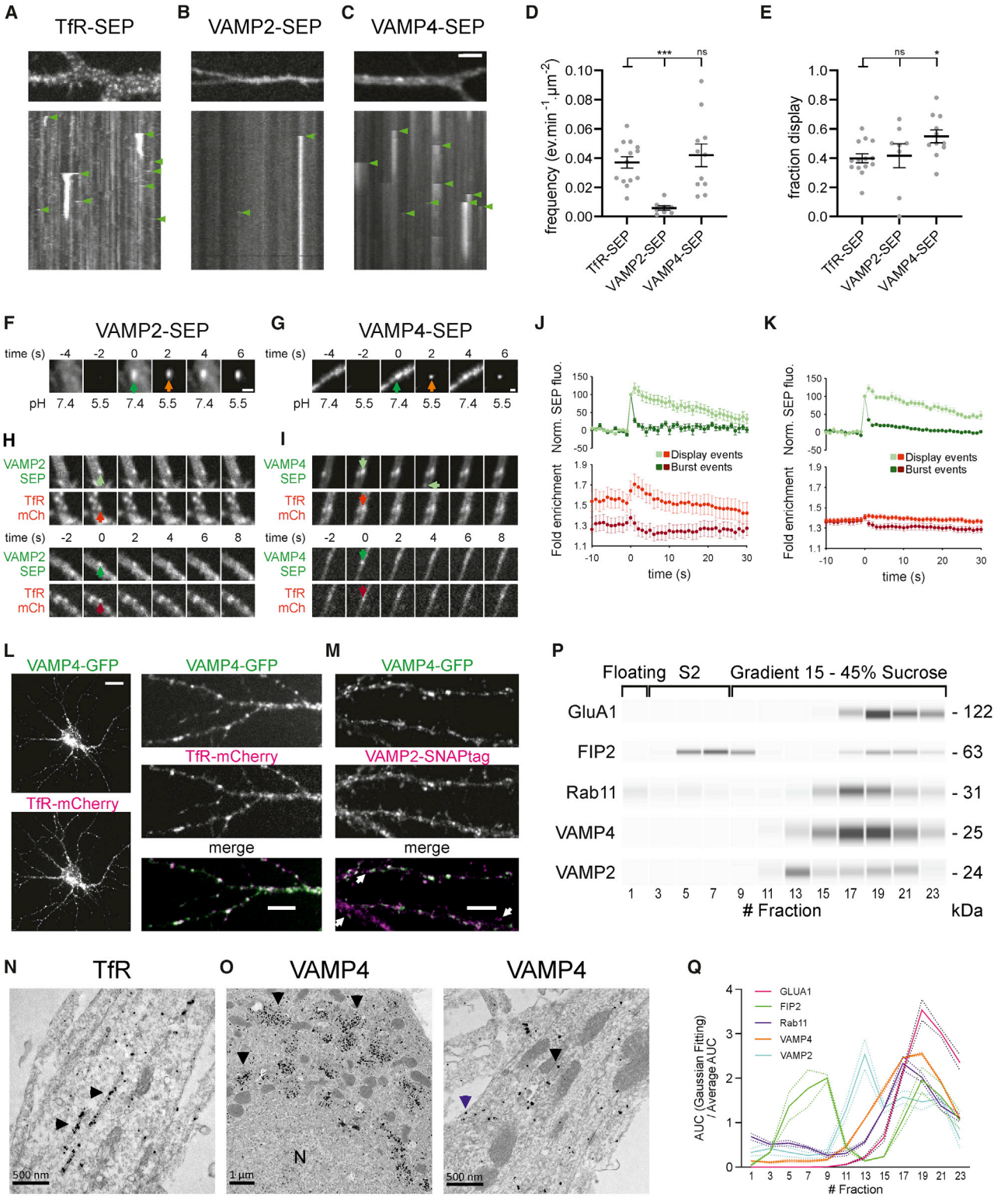

Figure 1. VAMP2 and VAMP4 are markers of recycling endosome exocytosis in the soma and dendrites of hippocampal neurons

(A–C) Images (top) and kymographs (bottom) of neurons (14 DIV) transfected with TfR-SEP (A), VAMP2-SEP (B), or VAMP4-SEP (C). Exocytosis events (sudden appearance of a bright cluster) are marked with green arrowheads. In (A), dim stable spots represent clathrin coated endocytic zones. Scale bar, 2 µm.

(legend continued on next page)

induction of LTP (Tanaka and Hirano, 2012; Yudowski et al., 2007). However, the rate of basal recycling and exocytosis differ between AMPARs and TfRs by almost an order of magnitude (Jullié et al., 2014; Temkin et al., 2017), and the term 'RE' possibly regroups a large diversity of organelles in neuronal dendrites that have not been deciphered yet (Kennedy and Ehlers, 2006; van der Sluijs and Hoogenraad, 2011). This large diversity of REs could use different proteins and regulators to undergo transport and fusion. One way to address this issue is to identify the molecular determinants of RE function.

The fusion step required for exocytosis is mediated by the cognate R- and Q-SNAREs, which are located on the vesicles and plasma membrane, respectively (Jahn and Scheller, 2006). Experiments using knockdown (KD) of individual SNARE proteins, together with electrophysiology, have identified SNAP47 and syntaxin-3 as the complementary Q-SNAREs necessary for the expression of LTP (Jurado et al., 2013). With the same strategy, complexin1 and -2 (Ahmad et al., 2012), as well as synaptotagmin1 and -7 (Wu et al., 2017), proteins involved in the calcium sensitivity of exocytosis (Brunger et al., 2019), were found to be necessary for the expression of LTP. Remarkably, KD of all these proteins (SNAP47, syntaxin3, complexin1 and -2, and synaptotagmin1 and -7) selectively affects LTP without affecting basal AMPAR- or NMDA receptor (NMDAR)-mediated synaptic transmission (Ahmad et al., 2012; Jurado et al., 2013; Wu et al., 2017). In contrast, the SNAREs and associated proteins mediating the constitutive recycling of AMPARs have remained elusive. The acute disruption of VAMP2 by clostridial toxins partially inhibits EPSCs (Lüscher et al., 1999; Penn et al., 2017; Wang et al., 2007). Moreover, surface localization of AMPARs is strongly reduced in cultured neurons from VAMP2 knockout (KO) mice, consistent with impaired recycling (Jurado et al., 2013). This suggests that AMPAR recycling is mediated, at least in part, by VAMP2. However, whether VAMP2 is necessary for all RE exocytosis events is still unknown.

Given the importance of somato-dendritic recycling in neuronal physiology, our goal was to identify major players in dendritic RE exocytosis. We found that the majority of RE fusion events labeled with TfR-SEP are mediated by VAMP4 and appear to be TeNT-insensitive, excluding a major contribution of VAMP2 in this pathway. The depletion of VAMP4 reduces TfR recycling but increases AMPAR recycling, presumably by blocking the retrograde trafficking of AMPARs to storage vesicles (SVs), leading to their missorting into a constitutive recycling pathway. Finally, we show, with patch-clamp recordings in organotypic hippocampal slices, that the increased surface localization of AMPARs is accompanied by an increased evoked EPSC in CA1 pyramidal cells and a partial occlusion of LTP.

RESULTS

VAMP4 is a marker of RE exocytosis in neuronal dendrites

The RE marker TfR-SEP reveals intense constitutive exocytosis activity in neuronal dendrites (Jullié et al., 2014; Kennedy et al., 2010; Roman-Vendrell et al., 2014). We measured a frequency of 0.037 ± 0.004 events.μm^{-2}.min^{-1} in cultured hippocampal neurons transfected with TfR-SEP and recorded at 13 to 15 *days in vitro* (DIV) with time-lapse spinning disk confocal microscopy at 1 Hz (Figure 1C; Video S1). We reasoned that other transmembrane RE proteins fused to SEP should report their exocytosis as well. In particular, vesicular SNAREs, essential proteins for the fusion step, are interesting candidates. When expressed in neurons, VAMP2-SEP is highly polarized to the axon, as previously shown (Sampo et al., 2003; Sankaranarayanan and Ryan, 2000) (see Figure 2B). In soma and dendrites, with comparatively low fluorescence, we recorded exocytosis events (Figure 1B; Video S2). However, the frequency of these events was only 0.0058 ± 0.0015 events.μm^{-2}.min^{-1}, much lower than the frequency of TfR-SEP events ($p = 0.0012$; Figure 1D). Therefore, VAMP2 is unlikely to be the only vSNARE responsible for TfR-SEP exocytosis. We then tested VAMP4 and VAMP7, other candidate vesicular SNAREs expressed in neurons. We could not detect exocytosis events in neurons transfected with

(D) Average frequency of exocytosis for neurons expressing TfR-SEP (n = 14), VAMP2-SEP (n = 8), or VAMP4-SEP (n = 11). All neurons were 13 to 15 DIV. Error bars represent SEM; ***p = 0.0012.
(E) Proportion of display events on the same sample as (D). Error bars represent SEM; **p < 0.01.
(F and G) Examples of events recorded in neurons transfected with VAMP2-SEP (F) and VAMP4-SEP (G) with the ppH protocol. After exocytosis (green arrow), a cluster resistant to low pH solution is clearly visible (orange arrow), demonstrating closure of the fusion pore within 4 seconds. Scale bars, 1 μm.
(H and I) Representative examples of exocytosis events recorded in neurons (14 DIV) expressing TfR-mCherry and VAMP2-SEP (H) or VAMP4-SEP (I). Upper panels show display events, and lower panel shows burst events. Green arrows indicate exocytosis sites, and red arrows show the corresponding TfR-mCherry clusters. Note that, for display events, TfR-mCherry clusters remain visible, whereas for burst events they largely disappear.
(J and K) Average normalized fluorescence curves for VAMP2-SEP (J, 59 display and 60 burst events in 8 cells) and VAMP4-SEP (K, 276 display and 394 burst events in 11 cells), together with TfR-mCherry fold enrichment (red curves). Light curves show display events and dark curves show burst events.
(L) Confocal microscopy images of a neuron (15 DIV) expressing VAMP4-GFP and TfR-mCherry. The somatic, peri-nuclear staining is saturated to enable the visualization of dendritic clusters. The higher magnification on the right shows clusters of VAMP-GFP co-localized with TfR-mCherry clusters. Scale bars, 10 μm (left) and 5 μm (right).
(M) Images of a neuron (14 DIV) expressing VAMP4-GFP and VAMP2-SNAPtag, incubated with 10 nM BG-JF646 for 30 min and imaged with confocal microscopy. Most clusters are colocalized, except for some VAMP2 clusters devoid of VAMP4 (white arrows). Scale bar, 5 μm.
(N) Silver-intensified immunogold labeling of endogenous TfR shows enrichment in dendritic tubular endosomal structures (arrows).
(O) Silver-intensified immunogold labeling of endogenous VAMP4. Labeling is enriched in the TGN (left, arrows) close to the nucleus (N). On a higher magnification view of a dendrite (right), VAMP4 is also found close to the membrane (blue arrow) and in endosomal compartments (black arrow) in dendrites.
(P) Immunodetection with WES of GluA1, FIP2, Rab11, VAMP4, and VAMP2 in microsomal fractions (S2) of hippocampus homogenates, initially in 10.9% sucrose, separated on a discontinuous gradient consisting of fractions ranging from 15% to 45% sucrose in 5% increments.
(Q) Quantification of abundance of the indicated protein (area under the curve [AUC]) in different fractions isolated in the sucrose gradient shown in (E). Graphs show the average ± SEM of three independent experiments normalized to average signal in all fractions.

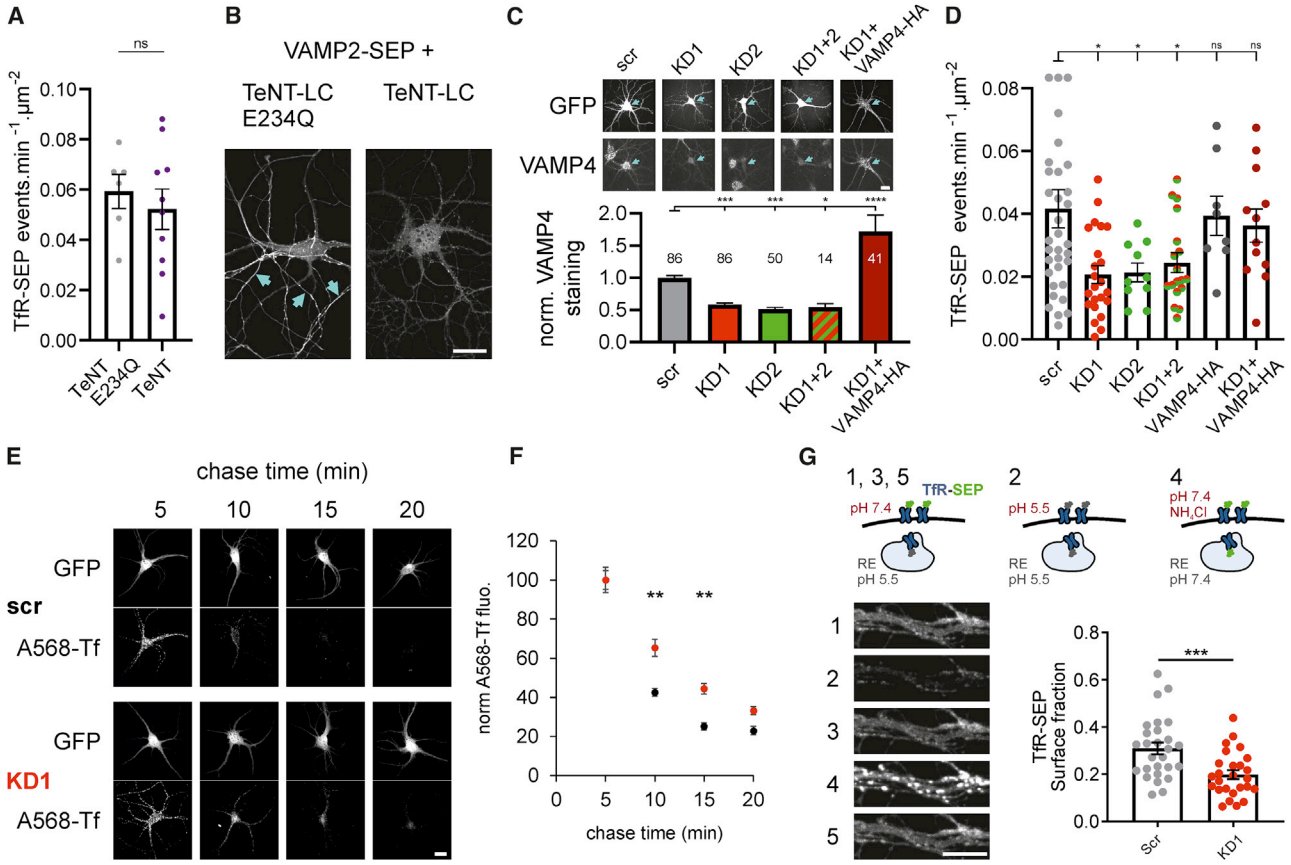

Figure 2. Downregulation of VAMP4, but not VAMP2, impairs RE exocytosis and recycling to the plasma membrane

(A) Frequency of exocytosis events in neurons transfected with TfR-SEP and TeNT-LC E234Q (n = 6) or TeNT-LC (n = 10).

(B) Images of neurons co-transfected with VAMP2-SEP and TeNT-LC E234Q or TeNT-LC. VAMP2-SEP is enriched in the axon (cyan arrows) in the first case but not the second case. Scale bar, 10 µm.

(C) Immunofluorescence images of endogenous VAMP4 in cells expressing GFP and a combination of shRNA targeted against VAMP4 for four days. In cells expressing GFP and the shRNA (cyan arrows), the labeling is strongly decreased compared to untransfected cells or cells expressing scramble (scr) shRNA. In cells co-expressing TfR, VAMP4-HA, and KD1, the VAMP4 staining is strong. Scale bar, 10 µm. Bottom, quantification of VAMP4 staining in the area delimited by the GFP mask (soma and dendrites). The staining is decreased by ~50% in all KD conditions. The number of cells is indicated above the bars for all conditions. Comparison with scr with one-way ANOVA; *p < 0.05 and ***p < 0.001.

(D) Frequency of exocytosis events recorded in cells expressing TfR-SEP and shRNAs targeted to VAMP4: scr (33 cells; 3 cells have frequencies of 0.132, 0.157, and 0.119 events.µm^{-2}.min^{-1} and are represented above the axis limit), KD1 (23 cells), KD2 (10 cells), KD1+2 (18 cells), cells expressing VAMP4-HA (8 cells), and KD1+VAMP4-HA (12 cells). *p < 0.05 one-way ANOVA.

(E) Images of neurons expressing scr or KD1 shRNAs in GFP vectors, labeled with A568-Tf (50 µg/ml) for 5 min and chased with unlabeled transferrin (2 mg/ml) at 37°C for the indicated times. Scale bar, 10 µm.

(F) Quantification of the Alexa568 fluorescence in the GFP mask from the pulse-chase experiments described in (E). 70 to 88 cells per condition from 4 independent experiments. Error bars represent SEM; **p < 0.01.

(G) Estimation of TfR-SEP surface fraction. Top, cartoons showing the fraction of fluorescent TfR-SEP. At pH 7.4, surface receptors are fluorescent, but not at pH 5.5. Receptors in acidic intracellular organelles are not fluorescent, but become fluorescent with NH_4Cl. Bottom left, images of a dendrite bathed successively in solutions at pH 7.4 (images 1, 3, and 5), pH 5.5 (image 2), and pH 7.4 containing NH_4Cl (image 4). For image 4, the contrast is 2× lower than in the other images. Bottom right, quantification of the TfR-SEP surface fraction for neurons transfected with scr (n = 27) and KD1 (n = 26). See STAR Methods for calculation. ***p < 0.001.

VAMP7-SEP at 15 DIV, even though exocytosis can be detected at earlier stages during neurite outgrowth (Burgo et al., 2012). In contrast, in neurons transfected with VAMP4-SEP, exocytosis events occur at a high frequency (0.042 ± 0.008 events.µm^{-2}.min^{-1}; n = 12; Figure 1C; Video S3), which is very similar to the frequency observed with TfR-SEP (one-way ANOVA; p = 0.77; Figure 1D).

RE exocytosis events in neuronal dendrites can be categorized into burst events, for which the membrane marker quickly diffuses into the plasma membrane, and display events, for which the RE remains visible for many seconds after rapid closure of the fusion pore (Hiester et al., 2017; Jullié et al., 2014; Roman-Vendrell et al., 2014). For both VAMP2 and VAMP4, the two types of events could be observed. The

proportion of display events was similar for TfR and VAMP2 and slightly higher for VAMP4 (one-way ANOVA; p = 0.97 and 0.06 for VAMP2 and VAMP4 versus TfR; Figure 1D). Alternating between pH 7.4 and 5.5 revealed that, like for TfR (Jullié et al., 2014), some display events are still visible after exchange with pH 5.5 solution (Figures 1F and 1G), hence report the transient opening of a fusion pore. Moreover, VAMP4-SEP exocytosis events occurred at TfR-mCherry clusters that label REs (Figure 1I), which is also the case for VAMP2-SEP exocytosis events (Figure 1H). The TfR-mCherry signal is stable after display exocytosis, while it decreases immediately after burst exocytosis (Figures 1H–1K), which is consistent with display exocytosis reporting a transient opening of a fusion pore. This behavior is similar to the one observed with TfR-SEP and other RE markers, such as internalized fluorescent Tf and Rab11a-mCherry (Jullié et al., 2014). RE exocytosis can be detected in the dendritic shaft but also in dendritic spines (Hiester et al., 2017; Kennedy et al., 2010). We detected occasional events in spines next to the PSD marker homer1c-tdTomato (Figure S1) (Rosendale et al., 2017), but the fraction of spine events was very small for both VAMP2-SEP events (0.8% ± 0.5% or 5/435 events recorded in 9 neurons) and VAMP4-SEP events (1.5% ± 0.4% or 12/1008 recorded in 8 neurons). We conclude from this data that VAMP2-SEP and VAMP4-SEP both mark the sites of RE exocytosis with very similar properties. However, the fact that VAMP4 reports about ten times more events than VAMP2 suggests that VAMP4 mediates most of the constitutive recycling in neuronal somato-dendritic compartments.

We examined the location of VAMP4 in dendrites in more detail. In neurons transfected with TfR-mCherry and VAMP4-GFP, where GFP is located in the cytoplasmic side of VAMP4 and thus visible in acidic intracellular compartments, the two markers are co-localized in the somato-dendritic compartment (Figure 1L). Both markers are highly enriched in a perinuclear compartment that corresponds to the trans-Golgi network (TGN), as seen in other cell types (Peden et al., 2001; Tran et al., 2007). In addition, clusters containing both proteins are visible along dendrites (Pearson's r 0.74 ± 0.03; n = 18). On the other hand, VAMP2-SNAPtag (labeled with benzylguanine-JF646) (Grimm et al., 2016) and VAMP4-GFP were also largely co-localized (Figure 1M) although to a smaller extent (Pearson's r 0.51 ± 0.02; n = 43). To get a better insight into the localization of VAMP4 in dendrites, we performed silver-intensified immunogold labeling of endogenous TfR and VAMP4 in thin sections of neurons observed with transmission electron microscopy. Labeling of TfR showed a clear accumulation of staining in tubular organelles, likely corresponding to REs (Figure 1N) (Cooney et al., 2002). Labeling of VAMP4 indicates that it is highly enriched in somatic perinuclear TGNs and is also found in dendritic tubular organelles (i.e., REs) (Figure 1O). Therefore, endogenous VAMP4 is present in dendritic REs and could participate in their exocytosis. As a complementary approach to determine whether VAMP2 and VAMP4 are in the same intracellular compartments, we performed subcellular fractionations of homogenized juvenile rat hippocampi and analyzed the presence of the RE marker Rab11, as well as the post-synaptic AMPAR subunit GluA1 and its associated protein FIP2 (Royo et al., 2019). Subcellular fractionation revealed the expected enrichment of the presynaptic VAMP2 and post-synaptic GluA1 in the crude synaptosome (P2) fraction, while VAMP4 was evenly distributed into crude synaptosomes (P2) and microsomes (S2) (Figure S2). Further fractionation of the microsomes on a discontinuous sucrose gradient showed the co-enrichement of VAMP4 and Rab11, further supporting the presence of VAMP4 in REs (Figures 1P and 1Q). GluA1 and FIP2 were most enriched in a slightly denser fraction, while VAMP2 was present in microsome populations: one similar to VAMP4/Rab11 and a lighter one (peak enrichment at fraction 13). We conclude that VAMP4 is present in REs located in dendrites and that VAMP2 may transit in REs but also accumulate in a less dense compartment.

Downregulation of VAMP4 but not cleavage of VAMP2 reduces TfR exocytosis and recycling

To determine the functional implication of VAMP2 and VAMP4 in RE exocytosis, we used molecular tools to suppress them or to block their action. VAMP2 and the closely related VAMP1 and VAMP3 are cleaved by TeNT (Binz et al., 2010), and expression of TeNT light chain (TeNT-LC) cleaves VAMP1-3 efficiently (Proux-Gillardeaux et al., 2005). VAMP3 is not expressed in hippocampal neurons (Schoch et al., 2001), while VAMP1 is expressed in the hippocampus specifically in interneurons late in development (Ferecskó et al., 2015; Vuong et al., 2018). Therefore, TeNT specifically targets VAMP2 in hippocampal pyramidal cells. However, the expression of TeNT-LC in neurons for 7 days did not affect the frequency of TfR-SEP exocytosis events compared to the co-expression of the inactive mutant TeNT-LC E234Q (Figure 2A). TeNT-LC was active because no exocytosis events could be recorded in neurons co-expressing VAMP2-SEP, while events could be recorded in neurons co-expressing the inactive mutant (0.0027 ± 0.0009 events.μm^{-2}.min^{-1}; n = 4). Moreover, TeNT-LC disrupted the polarized targeting of VAMP2-SEP to the axon (Figure 2B) and affected synaptic plasticity (see below). This indicates that the vast majority of the detected TfR-SEP exocytosis does not rely on the targets of TeNT, i.e., VAMP2.

We used a KD strategy with shRNAs to suppress the expression of VAMP4, as done before in neurons (Lin et al., 2020; Nicholson-Fish et al., 2015; Raingo et al., 2012). We selected two different shRNAs: KD1, which targets the 3′ UTR of VAMP4 mRNA, and KD2, which targets the coding sequence (see STAR Methods). As confirmed by immunofluorescence, co-transfection of either or both shRNAs with GFP for 4 to 5 days led to a strong decrease of the endogenous VAMP4 levels compared to the cotransfection with a scramble (scr) shRNA (Figure 2C). In addition, their expression reduces TfR-SEP exocytosis frequency by about 2-fold (Figure 2D). Co-expression of VAMP4-HA together with VAMP4 KD1 and TfR-SEP restored VAMP4 staining (Figure 2C) and the frequency of exocytosis events, while expression of VAMP4-HA alone did not affect event frequency (Figure 2D). This indicates that VAMP4 is involved in a fusion step necessary for the efficient recycling of TfR.

To directly test the involvement of VAMP4 in TfR recycling, we performed a pulse chase assay with Alexa568-labeled Tf (A568-Tf). After a 5 minute pulse and a 5 min chase with unlabeled holo-Tf, the amount of internalized A568-Tf was similar for neurons expressing KD1 in a GFP vector (1860 ± 180 AFU;

n = 74 neurons in 4 independent experiments) as in neurons expressing a scr shRNA in the GFP vector (2130 ± 161 AFU; n = 74 neurons in 4 independent experiments; unpaired t test p = 0.27) (Figure 2E). This suggests that TfR endocytosis is not impaired by VAMP4 KD. Moreover, in control conditions, TfR rapidly recycles to the cell surface, such that most A568-Tf is lost in 15 min. On the other hand, in neurons knocked down for VAMP4, the A568-Tf labeling is significantly higher after a 10- or 15-minute chase as compared to control (Figures 2E and 2F). This indicates that in spite of an efficient endocytosis, recycling of TfR at the cell surface is strongly delayed in these cells.

If recycling of TfR is selectively impaired, it should affect its steady-state localization between surface and intracellular pools. We measured the localization of TfR-SEP transfected in neurons first with an application of solution at pH 5.5 to reveal the proportion of surface receptors and then an application of ammonium solution at pH 7.4, which reveals the proportion of receptors in acidic intracellular compartments (Sankaranarayanan et al., 2000) (Figure 2G). As predicted, the surface fraction calculated from these measures was significantly smaller in neurons expressing KD1 (0.20 ± 0.02; n = 26 neurons) than in neurons expressing scr (0.30 ± 0.03; n = 27 neurons; unpaired t test p = 0.0008).

Both VAMP2 and VAMP4 exocytosis increase after cLTP

To study the regulated fusion of TfR-labeled REs in somato-dendritic regions, we performed a cLTP induction protocol (glycine 500 μM, 0 Mg^{2+}, 30 μM picrotoxin, and 10 μM strychnine for 5 min), which has been previously shown to enhance Tf recycling (Park et al., 2004), the surface fraction of TfR-SEP and the frequency of TfR-SEP exocytosis events in primary hippocampal cultures (Hiester et al., 2017; Keith et al., 2012; Kennedy et al., 2010). Indeed, in neurons transfected with TfR-SEP and cultured in Brainphys medium for 12 to 15 DIV (see STAR Methods), cLTP induces a robust and sustained increase in the frequency of exocytosis events (Figures 3A–3C; Video S4), which is maximal 15 min after cLTP induction (180% ± 21% of basal exocytosis frequency; n = 16 neurons). This increase is blocked by the NMDA receptor antagonist APV (100 μM) (91% ± 8%; n = 12 neurons), showing that this effect is due to the activation of NMDA receptors. In addition, cLTP induction increases dendrite fluorescence, which reflects the number of receptors at the cell surface (Hiester et al., 2017; Park et al., 2006), with a time course that matches the increase in exocytosis frequency (Figure 3D). The increase was maximal 20 min after cLTP induction (1.24 ± 0.04; n = 16; Figure 3E). The increase in fluorescence was also blocked by APV (Figures 3D and 3E) (0.99 ± 0.06; n = 12).

We then tested the same cLTP protocol in neurons transfected with VAMP2-SEP or VAMP4-SEP. For the two markers, the frequency of exocytosis events increased after cLTP induction and was maximal 15 min after induction (Videos S5 and S6). For VAMP2-SEP it was 235% ± 45% of basal exocytosis frequency (n = 9; paired t test p = 0.012) (Figures 3F–3H) and for VAMP4-SEP 201% ± 26% (n = 15 neurons; p = 0.002) (Figures 3K–3M). This increase was blocked by APV in both cases. Nevertheless, during cLTP induction and in the minutes after, the drop in frequency observed for all other conditions (Figures 3B, 3G, and 3L) and which may be due to a slight perturbation during exchange of solution (see STAR Methods), was not seen for VAMP2-SEP (Figure 3G), even though the increase was not significant compared to basal frequency. On the other hand, dendrite fluorescence of VAMP2-SEP increased immediately during cLTP induction and steadily in the 20 min after (Figure 3I), while it dropped initially and increased steadily for VAMP4-SEP fluorescence (Figure 3N). For both VAMP2-SEP and VAMP4-SEP, the increase was highly significant 20 min after cLTP induction (Figures 3J and 3O). Finally, the fluorescence increase was for both markers completely blocked by APV (0.95% ± 0.21%, n = 10 neurons; 0.98 ± 0.07, n = 10 neurons). Therefore, we conclude that the exocytosis of REs labeled with VAMP4-SEP or TfR-SEP is stimulated the same way by cLTP and likely corresponds to the same organelles.

Effect of TeNT and VAMP4 KD on RE exocytosis during cLTP induction

The expression of LTP, assessed by the increase in EPSC amplitude, is blocked by TeNT-LC (or BoNT-B) (Lledo et al., 1998; Lu et al., 2001; Penn et al., 2017). We tested the effect of TeNT-LC on the modulation of RE exocytosis during cLTP in somato-dendritic regions. Surprisingly, expression of TeNT-LC did not impair the increase in exocytosis frequency of TfR-SEP upon LTP induction (basal: 0.070 ± 0.017 events.μm^{-2}.min^{-1}; cLTP: 0.108 ± 0.020 events.μm^{-2}.min^{-1}, n = 13 neurons) compared to neurons expressing the inactive TeNT-LC E234Q (basal: 0.080 ± 0.064 events.μm^{-2}.min^{-1}; cLTP: 0.116 ± 0.075 events.μm^{-2}.min^{-1}, n = 13 neurons) (Figure 4A). Instead, TeNT-LC expression impaired the increase in surface fluorescence intensity of TfR-SEP (0.96 ± 0.05, n = 13 neurons) observed in the TeNT inactive control group (1.33 ± 0.08, n = 13 neurons) 20 min after LTP induction (Figures 4B–4D). These results suggest that VAMP2 does not mediate the regulated exocytosis of most REs in somato-dendritic compartments but is required for the stabilization of newly exocytosed receptors at the neuronal surface.

We then investigated the effect of VAMP4 KD on the exocytosis frequency of REs upon cLTP induction. Neurons were co-transfected with TfR-SEP and either scr or VAMP4 KD1 to downregulate VAMP4. Consistent with our previous results (Figure 2D), the basal frequency of TfR-SEP exocytosis event neurons in VAMP4 KD neurons was significantly reduced (0.047 ± 0.005 events.μm^{-2}.min^{-1}, n = 8 neurons) compared to scr neurons (0.146 ± 0.028 events.μm^{-2}.min^{-1}, n = 10 neurons, p = 0.005). Upon cLTP induction, TfR-SEP exocytosis frequency was increased in both scr neurons (0.232 ± 0.059 events.μm^{-2}.min^{-1}, n = 10 neurons, p = 0.003) and VAMP4 KD neurons (0.0653 ± 0.005 events.μm^{-2}.min^{-1}, n = 8 neurons, p = 0.014), although to a lesser extent (Figure 4E). This was accompanied by a significant increase in fluorescence intensity in scr (1.60 ± 0.19, n = 10 neurons) and VAMP4 KD neurons (1.56 ± 0.15, n = 9 neurons) (Figures 4F–4H). These results indicate that VAMP4 is necessary for basal RE exocytosis but is not required for the stimulation of TfR-SEP exocytosis during cLTP.

VAMP4 KD accelerates AMPAR recycling and impairs its modulation during LTP induction

We then asked if VAMP4 KD would have an effect on the dendritic insertion of AMPARs upon cLTP induction. In neurons

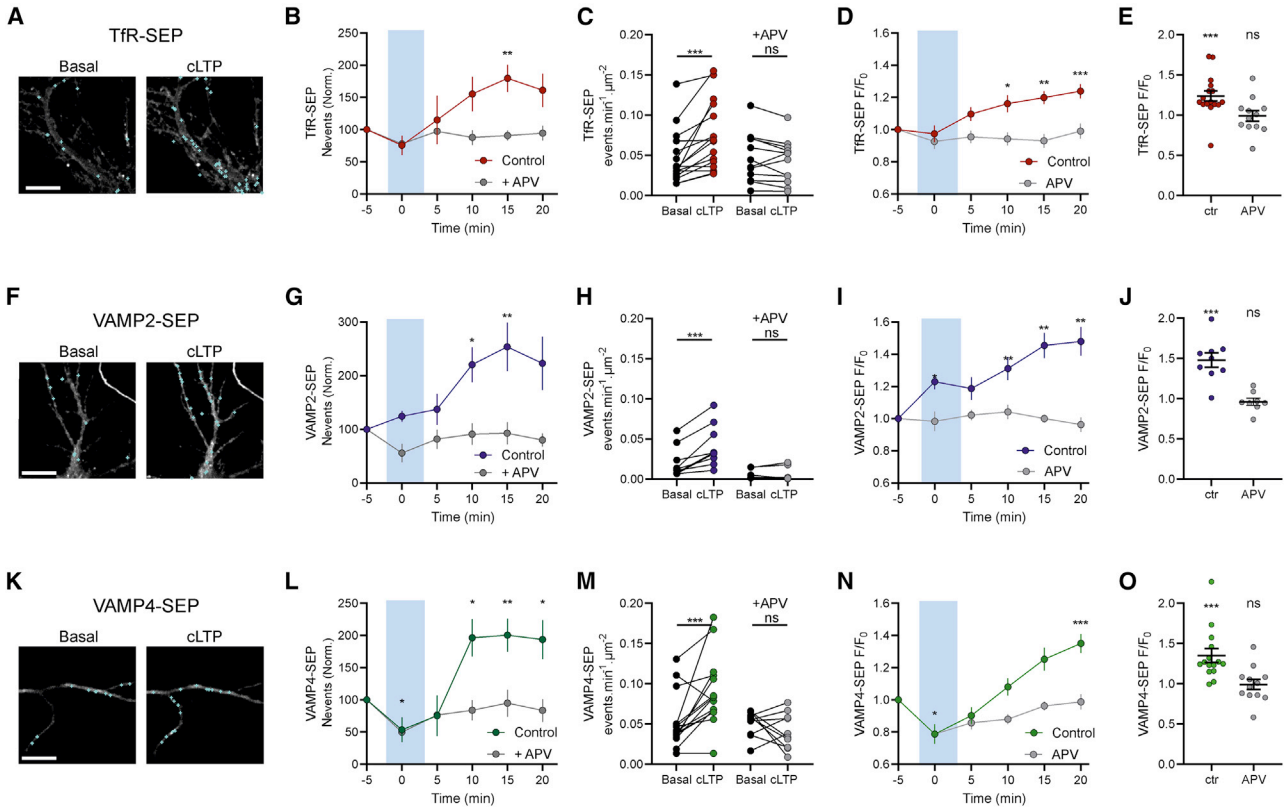

Figure 3. TfR-SEP and VAMP4-SEP exocytosis increase after chemical LTP

(A) Images of a neuron transfected with TfR-SEP before and 15 min after induction of cLTP. Cyan crosses show the location of detected exocytosis events. Scale bar, 5 µm.

(B) Normalized exocytosis frequency of neurons transfected with TfR-SEP at times relative to cLTP induction (n = 16, control [ctrl]). The light blue area denotes the time of incubation with cLTP inducing medium. The increase in frequency is significant 15 min after induction (Dunnett's multiple comparison test, p = 0.003). In the presence of APV (100 µM), the frequency does not increase (n = 12).

(C) Exocytosis frequencies before and 15 min after LTP induction. Paired t test p = 0.0008 (ctrl) and p = 0.14 (APV).

(D) Normalized change in fluorescence intensity of TfR-SEP before and after cLTP induction. The increase is significant after 10 min or more (Dunnett's multiple comparison).

(E) Changes in TfR-SEP fluorescence 20 min after cLTP induction, in ctrl (carmin dots) or with APV (gray dots). Paired t test p = 0.0002 (ctrl) and p = 0.89 (APV).

(F–J) Same as (A)–(E) for neurons transfected with VAMP2-SEP (n = 9) and with APV (n = 7). The increase in frequency is significant 10 min or more after induction (p = 0.002).

(K–O) Same as (A)–(E) for neurons transfected with VAMP4-SEP (n = 15) and with APV (n = 15). The increase in frequency is significant 15 min or more after induction (p = 0.0082).

transfected with the AMPAR subunit GluA1 tagged with SEP (SEP-GluA1) and either scr or VAMP4 KD1, we performed whole-cell fluorescence recovery after photobleaching for 25 min to measure the rate of insertion of SEP-GluA1 from intracellular acidic organelles, in which SEP is not fluorescent and hence not bleached (Temkin et al., 2017; Wu et al., 2017). Neurons were initially imaged and then photobleached immediately before cLTP induction (Figure 5A). In the control group (scr), the rate of SEP-GluA1 insertion was greatly increased after cLTP induction (16.2% ± 1.0% recovery after 25 min, n = 42) compared to block of cLTP induction with APV (5.9% ± 0.4%, n = 39, p < 0.0001) (Figure 5B). However, in neurons expressing VAMP4 KD1, cLTP did not change the rate of SEP-GluA1 recovery (cLTP: 6.8% ± 0.5%, n = 45 versus APV: 8.4% ± 0.6%, n = 41) (Figure 5C). On the other hand, the basal SEP-GluA1 recovery rate of VAMP4 KD neurons was significantly higher than that of control neurons (Figure 5D; p < 0.001). To further assess the effect of VAMP4 KD on the surface expression of SEP-GluA1, we measured the surface fraction of SEP-GluA1 by changing the pH of the perfusion buffer, similar to the experiment performed on TfR-SEP (Figure 2G). Indeed, the SEP-GluA1 surface fraction is significantly higher in VAMP4 KD compared to control (control: 0.53 ± 0.02, n = 15 neurons; VAMP4 KD: 0.62 ± 0.03, n = 15 neurons, p = 0.031) (Figure 5E). This contrasts with the reduction of TfR-SEP recycling and surface expression. Therefore, the depletion of VAMP4 affects the basal levels of plasma membrane AMPAR and TfR in an opposing manner. To confirm this surprising finding, we measured the frequency of exocytosis events in neurons expressing SEP-GluA1 with recordings at 1 Hz immediately after photobleaching (Figure 5F). Consistent

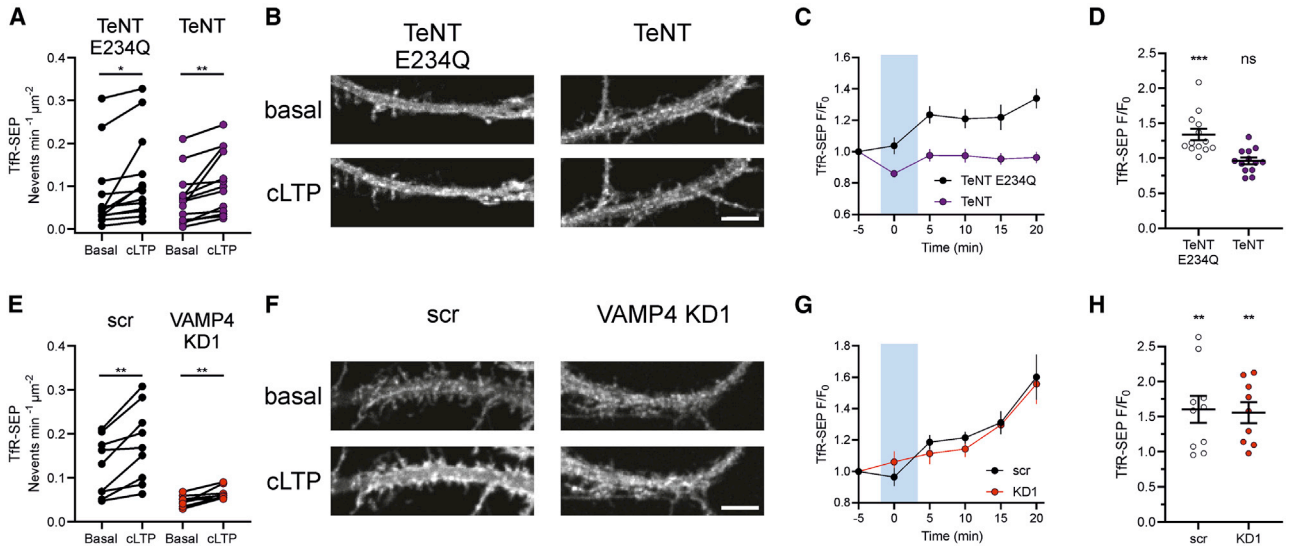

Figure 4. Effect of TeNT-LC and VAMP4 KD on TfR-SEP exocytosis after cLTP

(A) Exocytosis frequencies before and after LTP induction in neurons expressing TfR-SEP and either TeNT-LC E234Q (n = 13) or TeNT-LC (n = 13). In both conditions the increase in frequency is significant.

(B) Images of dendrites before and after induction of cLTP. Scale bar, 5 µm.

(C) TfR-SEP fluorescence in dendrites of neurons before and after cLTP induction.

(D–F) Same as (A)–(C) for neurons expressing TfR-SEP and either scr (n = 10) or VAMP4 KD1 (n = 8) shRNA.

with fluorescence recovery after photobleaching (FRAP) experiments, the frequency of exocytosis events was higher in neurons co-expressing SEP-GluA1 and VAMP4 KD1 (0.028 ± 0.004 events.μm^{-2}.min^{-1}) or KD2 (0.025 ± 0.005 events.μm^{-2}.min^{-1}) shRNAs than in neurons expressing scr shRNA (0.015 ± 0.002 events.μm^{-2}.min^{-1}; p = 0.0045 and 0.029, respectively). On the other hand, co-expression of SEP-GluA1 and TeNT-LC reduced the exocytosis event frequency from 0.013 ± 0.002 to 0.006 ± 0.001 events.μm^{-2}.min^{-1} compared to inactive TeNT-LC E234Q (Figure 5G; p = 0.0007). Finally, simultaneous expression of TeNT-LC and VAMP4 KD1 shRNA lowered the SEP-GluA1 exocytosis event frequency to the same extent as TeNT-LC alone (Figure 5H). These results show that AMPAR exocytosis depends on VAMP2, and that VAMP4 is necessary for the trafficking of AMPARs to a compartment that undergoes exocytosis after cLTP.

Effect of VAMP4 KD on synaptic transmission and plasticity

If VAMP4 KD affects AMPAR expression at the plasma membrane, it might affect synaptic transmission. To test this hypothesis, we first assessed the effect of VAMP4 KD on EPSCs evoked by Schaffer collateral stimulation (eEPSCs) in CA1 pyramidal neurons of hippocampal organotypic slices. We used lentiviral vectors to deliver KD1 and KD2 shRNAs against VAMP4 and a scr shRNA as a control. The degree of VAMP4 reduction in neurons transduced with lentivirus was about 50% in cultures, similar to the amount of KD obtained with plasmid transfection (Figure S3A). In addition, the high efficiency of lentiviral infection in cultures enabled us to quantify their effects with a western blot (Figure S3C). We found that VAMP4 expression (normalized to actin) was 41% ± 14% (KD1) and 5% ± 6% (KD2) relative to scr (three independent experiments), further validating these tools. We made simultaneous patch clamp recordings of eEPSCs from two neighboring CA1 pyramidal neurons, one transduced and the other not (Figures 6A and 6B). Expression of VAMP4 KD1 or KD2 enhanced AMPAR EPSCs by ~2-fold compared to neighboring, non-transduced neurons (Figures 6C and 6E) (KD1: 218% ± 36%, n = 14 pairs, KD2: 228% ± 36%, n = 12 pairs), while expression of scr had no effect (106% ± 20%, n = 17 pairs). Conversely, the NMDAR component of EPSCs recorded at +40 mV was unchanged in the scr, KD1, or KD2 conditions (Figures 6C and 6F). Consequently, the NMDA/AMPA ratio was reduced in KD cells compared to scr (Figure 6G). Despite the large effect of VAMP4 KD on AMPA mediated EPSCs, it did not affect spine density or length and led to a slight but significant increase in spine head size (Figure S4). The increase in AMPAR-EPSCs in VAMP4 KD cells is thus in line with the enhancement in GluA1 trafficking and surface expression detected in primary hippocampal cultures. We then tested the effect of TeNT-LC expression on synaptic transmission. We transfected individual CA1 pyramidal neurons by single-cell electroporation at 3 to 4 DIV and recorded neurons 3 to 4 days later. Neurons expressing TeNT-LC showed a reduction in both AMPAR (62% ± 10%, p = 0.0059) and NMDAR (63 ± 5, p = 0.043) EPSCs relative to control with no change in NMDA/AMPA ratio (Figures 6D and 6G) (n = 8 pairs).

Given the effect of VAMP4 KD on basal excitatory synaptic transmission, we wanted to test their effect on synaptic plasticity. NMDAR-dependent LTP was induced in hippocampal organotypic slices in the CA3-CA1 synapse using a standard pairing protocol of 100 stimulations at 1 Hz while holding the

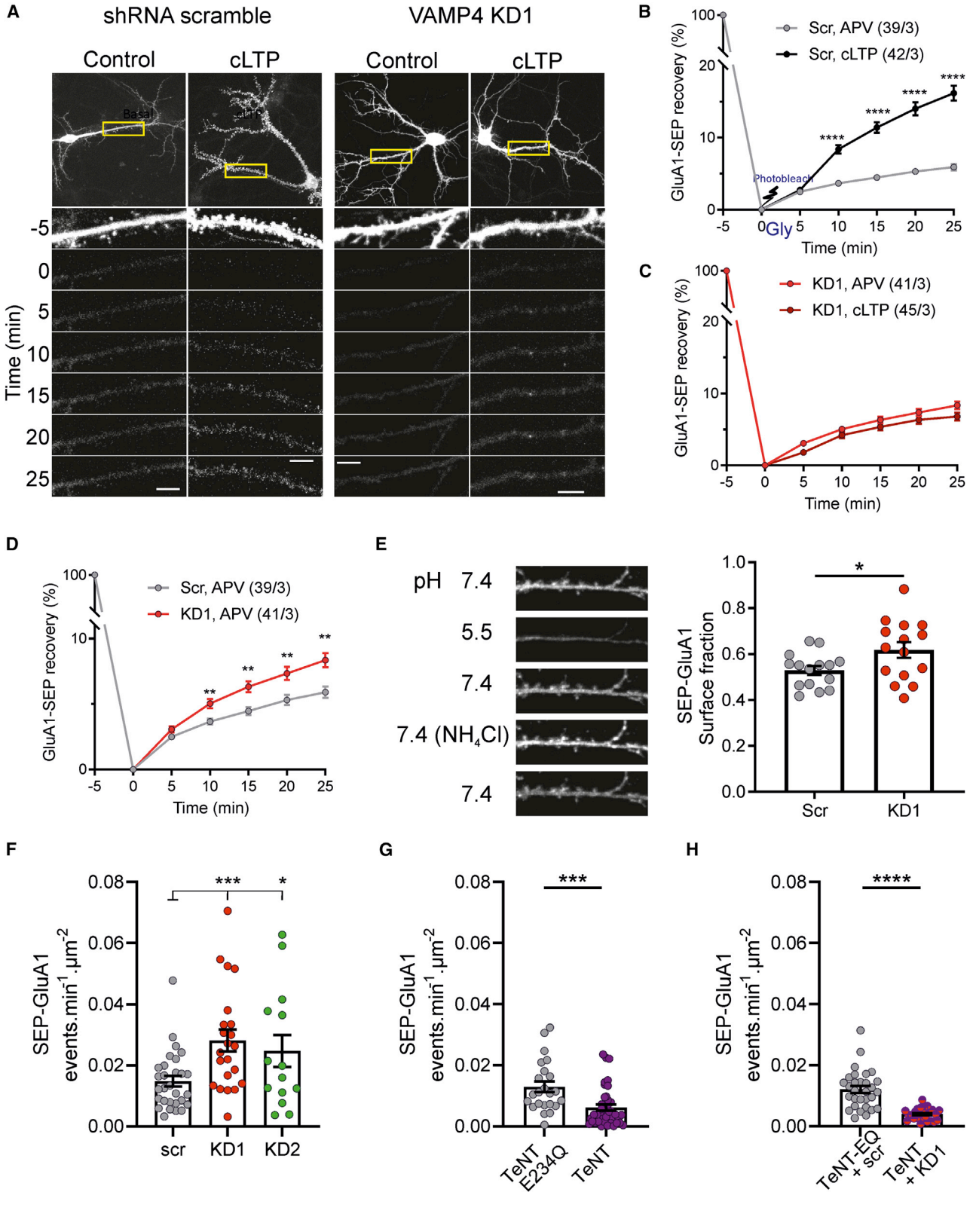

(legend on next page)

cell at 0 mV (Isaac et al., 1995). As expected, neurons expressing TeNT-LC showed no LTP, but rather a depression (62% ± 3%) compared to neighboring non-electroporated cells, which displayed normal LTP (274% ± 7%) (Figures 7A–7C). On the other hand, LTP was significantly reduced in neurons expressing VAMP4 KD1 (176% ± 9%) or KD2 (147% ± 6%), while neurons transduced with the scr shRNA lentivirus showed robust LTP (307% ± 10% of basal EPSC amplitude 20 to 30 min after induction) (Figures 7D–7F). Therefore, VAMP4 is important for basal synaptic transmission and could affect the magnitude of LTP by occluding further potentiation.

DISCUSSION

In the present study, we have investigated the role of two vSNARE proteins, VAMP2 and VAMP4, in both the constitutive and regulated endosomal trafficking at the post-synapse. Using a combination of live-cell imaging and electrophysiology techniques, we demonstrate that the exocytosis of TfR-labeled REs is mainly mediated by the TeNT-insensitive VAMP4. This vSNARE, classically involved in early endosome homotypic fusion and retrograde trafficking to the TGN (Brandhorst et al., 2006; Laufman et al., 2011; Mallard et al., 2002), is also involved in the endosomal sorting of AMPARs, whereas VAMP2 preferentially mediates AMPAR trafficking to the plasma membrane. These results support a model of a segregated endosomal recycling system at the post-synapse.

Involvement of VAMP4 in dendritic exocytosis

We have shown here that VAMP4 is the main vesicular SNARE involved in RE exocytosis in neuronal soma and dendrites. VAMP4-SEP co-localizes with TfR-mCherry, a classical RE marker, and reports the same frequency of exocytosis events as TfR-SEP, in the basal state or after cLTP induction. Moreover, VAMP4 KD decreases the frequency of TfR-SEP exocytosis events, the rate of Tfn recycling, and the fraction of TfR at the plasma membrane. In contrast, cleavage of VAMP2 by TeNT-LC does not affect the frequency of exocytosis events in neuronal dendrites.

VAMP4 has been implicated in other exocytosis processes in neurons. In presynaptic terminals, in addition to VAMP2, the main SNARE mediating calcium-dependent synaptic vesicle exocytosis (Schoch et al., 2001), VAMP4 is responsible for the exocytosis of vesicles that mediate so-called asynchronous exocytosis (Raingo et al., 2012). It forms a complex with syntaxin-1 and SNAP-25, the other SNAREs classically involved in synaptic vesicle exocytosis together with VAMP2 (Jahn and Scheller, 2006). Interestingly, the SNARE complex formed by VAMP4, syntaxin-1, and SNAP-25 does not bind complexins or synaptotagmin-1 (Raingo et al., 2012), proteins involved in the calcium-dependent synchronous exocytosis of synaptic vesicles (Brunger et al., 2019). Moreover, VAMP4 is involved in an endocytic process, the activity-dependent bulk endocytosis (Nicholson-Fish et al., 2015) which participate in the recycling of synaptic vesicles. Lastly, VAMP4 has been implicated in the exocytosis of organelles called enlargeosomes, which are responsible for fast neurite outgrowth in the neuroendocrine cell line PC12-27, as well as in primary neurons (Borgonovo et al., 2002; Cocucci et al., 2008). Until now, even though VAMP4 is primarily located in the somato-dendritic compartment of hippocampal neurons (Jain et al., 2015, no specific role was assigned to VAMP4 in dendritic membrane trafficking. We show here that VAMP4 has a major role in RE exocytosis in neuronal soma and dendrites. Nevertheless, VAMP2 is also involved in dendritic exocytosis of a subset of REs labeled with TfR-mCherry. Because the frequency of VAMP2-SEP exocytosis events represents only about 13% of the frequency of VAMP4-SEP exocytosis events, the quantitative role of VAMP2 in recycling is minor, which explains why TeNT-LC does not detectably affect the frequency of TfR-SEP exocytosis events. However, specific cargo may travel through VAMP2 dependent vesicles. In particular, we confirm that the exocytosis of the AMPAR subunit GluA1 is blocked by TeNT (Lin et al., 2009). Other subunits of post-synaptic receptors, such as GluA2 or the $GABA_AR$ subunit $\gamma 2$, are sensitive to TeNT-LC or to VAMP2 KD (Gu et al., 2016). Consistent with the role of VAMP2 in post-synaptic receptor exocytosis, we show that chronic expression of TeNT-LC decreases eEPSC amplitude and completely blocks LTP, as does acute block during recording (Lledo et al., 1998; Lu et al., 2001; Penn et al., 2017).

VAMP4 is necessary for endosomal sorting of AMPARs

In addition to largely inhibiting RE exocytosis, KD of VAMP4 also increases GluA1 exocytosis and the fraction of surface receptors. Consistent with this effect, the amplitude of EPSCs mediated by AMPARs is increased in VAMP4 KD neurons. This effect is opposite to the one on TfR trafficking and points to a second function of VAMP4 that is distinct from RE exocytosis. Effectively, the most documented role of VAMP4 in cells is in the so-called retrograde transport from early endosomes to the TGN (Laufman et al., 2011; Mallard et al., 2002), which corresponds to its main localization in TGN of neurons (this

Figure 5. VAMP4 regulates the recycling of AMPA receptors and its availability for cLTP

(A) Images of neurons expressing SEP-GluA1 and either scr or VAMP4 KD1 shRNA. Images are maximum projections of stacks of nine planes. Below, images of the dendrite framed in yellow before and at the indicated time after photobleaching of the whole cell. Scale bars, 5 μm. Images before bleaching are displayed saturated to keep the same contrast as the ones after bleaching.

(B–D) Quantification of SEP-GluA1 fluorescence in dendritic segments, normalized to pre- and post-bleach values. Cells were kept if the total fluorescence was bleached by more than 90%.

(B) Neurons expressing scr shRNA with glycine treatment for cLTP or APV.

(C) Neurons expressing VAMP4 KD1 shRNA with glycine treatment for cLTP or APV.

(D) The two conditions of (B) and (C) in APV are replotted with a higher scale to highlight the difference between the two recovery rates.

(E) Images of a dendritic segment of a neuron transfected with SEP-GluA1 and scr shRNA, following the same protocol as described in Figure 3G. Right, quantification of SEP-GluA1 surface fraction in neurons expressing scr (n = 15) or VAMP4 KD1 shRNA (n = 15).

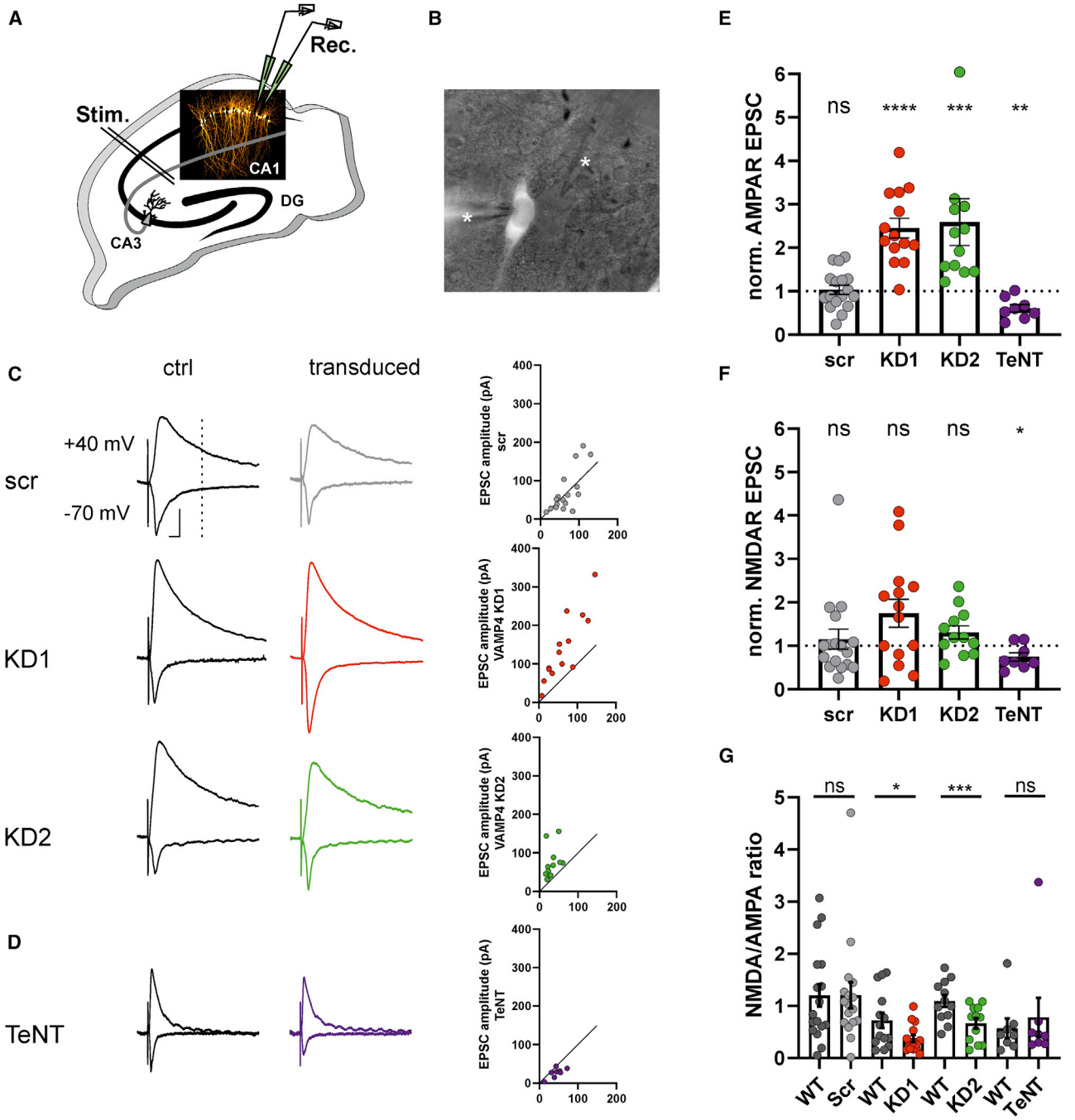

Figure 6. Effect of post-synaptic VAMP4 KD and TeNT on glutamatergic synaptic transmission

(A) Confocal image of an organotypic hippocampal slice culture infected with scr-mScarlet lentivirus at 1 DIV and fixed at 9 DIV. Many pyramidal neurons in CA1 are brightly fluorescent.

(B) DIC image of two pyramidal neurons recorded simultaneously with patch pipettes (asterisks). Epifluorescent illumination shows that the neuron on the left is brightly fluorescent (infected) while the one on the right is not (uninfected control).

(C) Averages of 30 EPSCs evoked by the same stimulation in pairs of neurons, uninfected and infected with scr-mScarlet (top), shRNA KD1-mScarlet (middle), or shRNA KD2-mScarlet (botttom). Both neurons were held at −70 mV then at +40 mV. Right, plots of peak EPSC amplitude at −70 mV for each pair of neurons. In the scr condition, dots are spread around the diagonal, while in the KD1 and KD2 conditions the amplitudes are systematically higher for infected neurons.

(D) Same as (C) for neurons co-electroporated with TeNT-LC and GFP. In the neurons expressing TeNT-LC, the amplitude is sytematically smaller than in control neurons.

(legend continued on next page)

study) and other cell types (Peden et al., 2001; Tran et al., 2007). The retrograde trafficking is mediated by the formation of tubulo-vesicular carriers in early endosomes by the retromer complex composed of the core subunits Vps26a,b/29/35 (Burd and Cullen, 2014). In neurons, this complex also mediates direct recycling of cargo, such as β2 adrenergic receptors or AMPARs, to the plasma membrane through the retromer-associated protein SNX27 (Hussain et al., 2014; Lauffer et al., 2010). Subunits of the retromer complex are present throughout dendrites next to early endosomal markers such as EEA1 (Choy et al., 2014). KD of the retromer core subunit Vps35 inhibits AMPAR recycling in neurons in culture and LTP in CA1 pyramidal neurons in slices (Temkin et al., 2017). Interestingly, in differentiated 3T3-L1 adipocytes, formation and stability of SVs containing the glucose transporter GLUT4 (GSVs) (Leto and Saltiel, 2012) depend on the retromer complex (Pan et al., 2017). Moreover, GSV exocytosis, which is elicited by stimulation with insulin, specifically depends on VAMP2, while VAMP4 controls the targeting of GLUT4 to GSVs: after VAMP4 KD GLUT4 exocytosis largely occurs without stimulation (Williams and Pessin, 2008), a phenotype similar to the one observed here in neurons for GluA1. Therefore, control of AMPARs exocytosis in neurons or GLUT4 exocytosis in adipocytes could share common pathways.

Based on these results, we can draw a model of dendritic recycling in neuronal dendrites (Figure 7G). After internalization into early endosomes, receptor cargo is sorted in at least two endosomal compartments. The majority of compartments are composed of Res, which are formed independently of retromer and contain TfRs. Their exocytosis is mediated by VAMP4, possibly interacting with cognate SNAREs involved in exocytosis, such as the dendritic syntaxins 3 or 4 (Arendt et al., 2015; Jurado et al., 2013; Kennedy et al., 2010). A second type of compartment, which we call ARV (AMPAR recycling vesicle), depends on the retromer complex for its formation. We suggest that ARVs are subject to more regulation than conventional REs, which seem to recycle back to the plasma membrane by default. Particularly, ARVs use VAMP4 to mature into a storage compartment containing AMPARs, AMPAR SV (ASV), which uses VAMP2 for exocytosis. To perform this function, VAMP4 could interact with cognate SNAREs involved in intracellular fusion steps such as syntaxin 6 and 13, individually or in combination (Koike and Jahn, 2019). In the absence of VAMP4, the ARV does not mature into an ASV and is recycled to the plasma membrane, enhancing the speed of AMPAR recycling but decreasing the capacity of the cell to potentiate after LTP induction. This provides a mechanistic explanation as to why, in the absence of VAMP4, AMPAR exocytosis is not enhanced during cLTP in cultured neurons and synaptic LTP is partially occluded by already potentiated synapses. ASVs could contain FIP2, initially characterized as an effector of Rab11 and potential mediator of RE movement through interaction with myosin V (Wang et al., 2008) but recently re-characterized as mediating the intracellular retention of AMPARs through direct binding (Royo et al., 2019). Interestingly, FIP2 KD decreases the fraction of TfR at the neuronal surface and increases the surface fraction of GluA1, a phenotype similar to the one we describe here with VAMP4 KD. Moreover, upon LTP induction, FIP2 is dephosphorylated and dissociates from AMPARs, freeing the cargo to translocate to the plasma membrane and undergo exocytosis (Royo et al., 2019). More research would be required to characterize the ASV and its behavior after the induction of LTP.

A sequence of fusion events for the expression of LTP

LTP-inducing stimuli enhance the overall endocytic recycling to the plasma membrane in hippocampal neurons (Park et al., 2004). The induction of cLTP in primary cultures causes an increase in TfR-SEP exocytosis frequency and surface fluorescence intensity, as previously reported (Hiester et al., 2017; Keith et al., 2012; Kennedy et al., 2010). Our results show that VAMP2-SEP and VAMP4-SEP exhibit similar behaviors to that of TfR-SEP upon cLTP induction, with VAMP2-SEP mediating an immediate response, while the VAMP4-SEP increase is delayed (Figure 3). However, even though VAMP4 KD reduced basal TfR recycling, cLTP induction similarly increased in proportion the TfR-SEP exocytosis frequency and surface fluorescence intensity. The residual regulated fusions might be due to the partial KD of VAMP4 or the existence of other TfR-positive REs that are mediated by a different vSNARE (e.g., VAMP2). In all cases, these data show that VAMP4 mediates the majority of TfR-labeled REs' basal and regulated exocytosis during LTP expression.

In contrast, expression of TeNT-LC had no effect on the basal exocytosis frequency of TfR-SEP. Moreover, it did not prevent the increase in frequency after cLTP induction, excluding a major contribution of VAMP2 in mediating RE fusion events. However, VAMP2 cleavage by TeNT-LC abolished the accompanied increase in TfR-SEP fluorescence intensity, as observed previously (Hiester et al., 2018). These results strongly suggest that the TeNT-LC effect on surface TfR-SEP is not caused by a general block of activity-triggered RE fusion but rather due to a failure to stabilize newly exocytosed receptors at the plasma membrane. One possibility is that VAMP2 mediates the exocytosis of a yet unidentified molecule that is necessary for the stabilization of surface receptors for LTP expression. Interestingly, the VAMP2-SEP increase in frequency following cLTP induction has an immediate component, unlike VAMP4-SEP or TfR-SEP (which reflects mostly VAMP4-contaning REs), suggesting that exocytosis of this factor is an early event in LTP expression. Factors released during cLTP induction, which are sensitive to TeNT-LC, could include brain-derived neurotrophic factors (BDNFs) (Harward et al., 2016) or other factors not yet identified. This goes in line with a study showing that TeNT-LC prevented the stabilization of AMPARs initially recruited with activity to

(E) Peak EPSC amplitude recorded at −70 mV (AMPAR component) normalized to the corresponding controls (uninfected, gray dots).
(F) EPSC amplitude 100 ms after stimulation at +40 mV (NMDAR component), normalized to the corresponding controls (uninfected, gray dots).
(G) Ratio of NMDAR/AMPAR EPSC amplitude for all conditions.
(E)–(G) Stars signal significant differences (paired t test, *$p < 0.05$, **$p < 0.01$, ***$p < 0.001$)

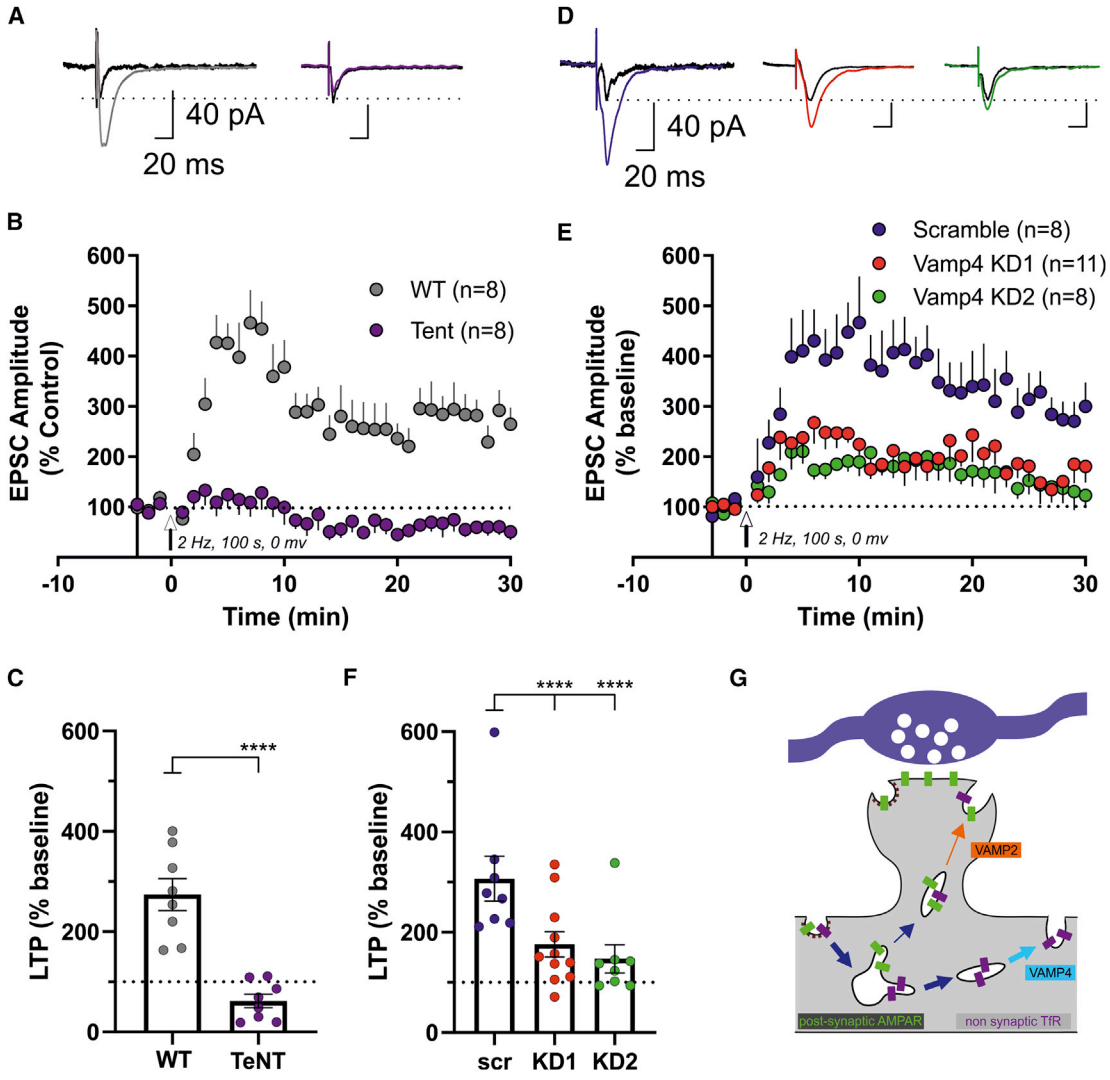

Figure 7. Effect of post-synaptic VAMP4 KD and TeNT on LTP

(A) Average EPSCs before (black traces) and 20 to 30 min after induction of LTP (color traces) in neurons electroporated with GFP and TeNT-LC (purple) or not (gray). The dotted line shows the peak EPSC before LTP induction. Scale bars, 40 pA and 20 ms.

(B) Peak EPSC amplitude normalized to baseline for pairs of neurons transfected with TeNT-LC (purple) or not (gray)

(C) Ratio of EPSC amplitude 20 to 30 min after LTP induction to baseline.

(D) Same as (A) for neurons transduced with lentivirus expressing scr-mScarlet (blue), shRNA KD1-mScarlet (red), and shRNA KD2-mScarlet (green). Scale bars, 40 pA and 20 ms.

(E) Peak EPSC amplitude normalized to baseline for of neurons expressing the corresponding shRNAs.

(F) Same as (C) for transduced neurons. ****$p < 0.0001$.

(G) Model of dendritic TfR and AMPAR receptor trafficking.

spines by lateral diffusion (Hiester et al., 2018). Altogether, this observation reinstates the importance of membrane exocytosis for the maintenance of surface receptors after LTP-inducing stimuli, seemingly regardless of their trafficking site (Choquet, 2018).

In conclusion, our study identifies VAMP4 as a major player in the post-synaptic SNARE fusion machinery that mediates most TfR-labeled RE fusions. In addition, VAMP4 controls the sorting of AMPARs into ASVs, which can be mobilized upon LTP induction. This represents an additional trafficking route of AMPARs for LTP expression. Yet, the precise sequence of various trafficking events and the specific organelles involved during the expression of LTP awaits further investigation.

STAR★METHODS

Detailed methods are provided in the online version of this paper and include the following:

- KEY RESOURCE TABLE

SUPPLEMENTAL INFORMATION

Supplemental information can be found online at https://doi.org/10.1016/j.celrep.2021.109678.

ACKNOWLEDGMENTS

We thank the IINS cell biology facility for neuronal cultures, Axel Athané for help with molecular biology, Sophie Daburon for biochemistry, and Christel Poujol and Sébastien Marais of the Bordeaux Imaging Center (member of France BioImaging supported by the Agence Nationale pour la Recherche; ANR-10-INBS-04) for help with spinning disk confocal microscopy. The work was supported by the Centre National de la Recherche Scientifique (PEPS & Interface programs) and the Agence Nationale pour la Recherche (CaPeBIE ANR-12-BSV5-005 and LocalEndoProbes ANR-17-CE16-0012) to D.P.; the Erasmus Mundus ENC program and the Labex BRAIN extension grant (ANR-10-LABX-43 BRAIN) to J.K.; and the European Union (Syndegen Initial Training Network) and the Labex BRAIN extension grant to M.B.

AUTHOR CONTRIBUTIONS

M.B. performed cLTP live cell imaging experiments and most slice electrophysiology experiments and analyzed the corresponding data. D.J. performed most live cell imaging in basal conditions and analyzed the corresponding data. J.K. performed some live cell imaging, immunocytochemistry, and electrophysiology experiments. V.P.-B. and E.H. performed subcellular fractionation and WES experiments. L.B. validated the VAMP4 shRNAs with immunofluorescence and western blot. J.P. performed electron microscopy experiments. N.R. and C.B. made and validated plasmids. D.C. provided essential support and guidance. D.P. conceived the study, curated all data, and wrote the article. All authors edited the manuscript.

DECLARATION OF INTERESTS

The authors declare no competing interests.

Received: December 3, 2020
Revised: June 25, 2021
Accepted: August 17, 2021
Published: September 7, 2021

REFERENCES

Ahmad, M., Polepalli, J.S., Goswami, D., Yang, X., Kaeser-Woo, Y.J., Südhof, T.C., and Malenka, R.C. (2012). Postsynaptic complexin controls AMPA receptor exocytosis during LTP. Neuron *73*, 260–267.

Arendt, K.L., Zhang, Y., Jurado, S., Malenka, R.C., Südhof, T.C., and Chen, L. (2015). Retinoic Acid and LTP Recruit Postsynaptic AMPA Receptors Using Distinct SNARE-Dependent Mechanisms. Neuron *86*, 442–456.

Bardy, C., van den Hurk, M., Eames, T., Marchand, C., Hernandez, R.V., Kellogg, M., Gorris, M., Galet, B., Palomares, V., Brown, J., et al. (2015). Neuronal medium that supports basic synaptic functions and activity of human neurons in vitro. Proc. Natl. Acad. Sci. USA *112*, E2725–E2734.

Bentley, M., and Banker, G. (2016). The cellular mechanisms that maintain neuronal polarity. Nat. Rev. Neurosci. *17*, 611–622.

Bindels, D.S., Haarbosch, L., van Weeren, L., Postma, M., Wiese, K.E., Mastop, M., Aumonier, S., Gotthard, G., Royant, A., Hink, M.A., and Gadella, T.W., Jr. (2017). mScarlet: a bright monomeric red fluorescent protein for cellular imaging. Nat. Methods *14*, 53–56.

Binz, T., Sikorra, S., and Mahrhold, S. (2010). Clostridial neurotoxins: mechanism of SNARE cleavage and outlook on potential substrate specificity reengineering. Toxins (Basel) *2*, 665–682.

Borgonovo, B., Cocucci, E., Racchetti, G., Podini, P., Bachi, A., and Meldolesi, J. (2002). Regulated exocytosis: a novel, widely expressed system. Nat. Cell Biol. *4*, 955–962.

Brandhorst, D., Zwilling, D., Rizzoli, S.O., Lippert, U., Lang, T., and Jahn, R. (2006). Homotypic fusion of early endosomes: SNAREs do not determine fusion specificity. Proc. Natl. Acad. Sci. USA *103*, 2701–2706.

Brown, T.C., Correia, S.S., Petrok, C.N., and Esteban, J.A. (2007). Functional compartmentalization of endosomal trafficking for the synaptic delivery of AMPA receptors during long-term potentiation. J. Neurosci. *27*, 13311–13315.

Brunger, A.T., Choi, U.B., Lai, Y., Leitz, J., White, K.I., and Zhou, Q. (2019). The pre-synaptic fusion machinery. Curr. Opin. Struct. Biol. *54*, 179–188.

Burd, C., and Cullen, P.J. (2014). Retromer: a master conductor of endosome sorting. Cold Spring Harb. Perspect. Biol. *6*, a016774.

Burgo, A., Proux-Gillardeaux, V., Sotirakis, E., Bun, P., Casano, A., Verraes, A., Liem, R.K.H., Formstecher, E., Coppey-Moisan, M., and Galli, T. (2012). A molecular network for the transport of the TI-VAMP/VAMP7 vesicles from cell center to periphery. Dev. Cell *23*, 166–180.

Choquet, D. (2018). Linking Nanoscale Dynamics of AMPA Receptor Organization to Plasticity of Excitatory Synapses and Learning. J. Neurosci. *38*, 9318–9329.

Choy, R.W.-Y., Park, M., Temkin, P., Herring, B.E., Marley, A., Nicoll, R.A., and von Zastrow, M. (2014). Retromer mediates a discrete route of local membrane delivery to dendrites. Neuron *82*, 55–62.

Cocucci, E., Racchetti, G., Rupnik, M., and Meldolesi, J. (2008). The regulated exocytosis of enlargeosomes is mediated by a SNARE machinery that includes VAMP4. J. Cell Sci. *121*, 2983–2991.

Cooney, J.R., Hurlburt, J.L., Selig, D.K., Harris, K.M., and Fiala, J.C. (2002). Endosomal compartments serve multiple hippocampal dendritic spines from a widespread rather than a local store of recycling membrane. J. Neurosci. *22*, 2215–2224.

Correia, S.S., Bassani, S., Brown, T.C., Lisé, M.-F., Backos, D.S., El-Husseini, A., Passafaro, M., and Esteban, J.A. (2008). Motor protein-dependent transport of AMPA receptors into spines during long-term potentiation. Nat. Neurosci. *11*, 457–466.

Costes, S.V., Daelemans, D., Cho, E.H., Dobbin, Z., Pavlakis, G., and Lockett, S. (2004). Automatic and quantitative measurement of protein-protein colocalization in live cells. Biophys. J. *86*, 3993–4003.

De-Smedt-Peyrusse, V., Darriet, L., Trifilieff, P., Herzog, E., and Angelo, M.F. (2018). Subcellular Fractionation of Brain Tissue from Small Tissue Explants, K.M.M. Synaptosomes, ed. (Springer), pp. 75–84.

Ehlers, M.D. (2000). Reinsertion or degradation of AMPA receptors determined by activity-dependent endocytic sorting. Neuron *28*, 511–525.

Ferecskó, A.S., Jiruska, P., Foss, L., Powell, A.D., Chang, W.-C., Sik, A., and Jefferys, J.G.R. (2015). Structural and functional substrates of tetanus toxin in an animal model of temporal lobe epilepsy. Brain Struct. Funct. *220*, 1013–1029.

Glebov, O.O., Tigaret, C.M., Mellor, J.R., and Henley, J.M. (2015). Clathrin-independent trafficking of AMPA receptors. J. Neurosci. *35*, 4830–4836.

Gordon, D.E., Bond, L.M., Sahlender, D.A., and Peden, A.A. (2010). A targeted siRNA screen to identify SNAREs required for constitutive secretion in mammalian cells. Traffic *11*, 1191–1204.

Granger, A.J., and Nicoll, R.A. (2013). Expression mechanisms underlying long-term potentiation: a postsynaptic view, 10 years on. Philos. Trans. R. Soc. Lond. B Biol. Sci. *369*, 20130136.

Grimm, J.B., English, B.P., Choi, H., Muthusamy, A.K., Mehl, B.P., Dong, P., Brown, T.A., Lippincott-Schwartz, J., Liu, Z., Lionnet, T., and Lavis, L.D. (2016). Bright photoactivatable fluorophores for single-molecule imaging. Nat. Methods *13*, 985–988.

Gu, Y., Chiu, S.-L., Liu, B., Wu, P.-H., Delannoy, M., Lin, D.-T., Wirtz, D., and Huganir, R.L. (2016). Differential vesicular sorting of AMPA and $GABA_A$ receptors. Proc. Natl. Acad. Sci. USA *113*, E922–E931.

Harward, S.C., Hedrick, N.G., Hall, C.E., Parra-Bueno, P., Milner, T.A., Pan, E., Laviv, T., Hempstead, B.L., Yasuda, R., and McNamara, J.O. (2016). Autocrine BDNF-TrkB signalling within a single dendritic spine. Nature *538*, 99–103.

Hiester, B.G., Bourke, A.M., Sinnen, B.L., Cook, S.G., Gibson, E.S., Smith, K.R., and Kennedy, M.J. (2017). L-Type Voltage-Gated Ca^{2+} Channels Regulate Synaptic-Activity-Triggered Recycling Endosome Fusion in Neuronal Dendrites. Cell Rep. *21*, 2134–2146.

Hiester, B.G., Becker, M.I., Bowen, A.B., Schwartz, S.L., and Kennedy, M.J. (2018). Mechanisms and Role of Dendritic Membrane Trafficking for Long-Term Potentiation. Front. Cell. Neurosci. *12*, 391.

Huganir, R.L., and Nicoll, R.A. (2013). AMPARs and synaptic plasticity: the last 25 years. Neuron *80*, 704–717.

Hussain, N.K., Diering, G.H., Sole, J., Anggono, V., and Huganir, R.L. (2014). Sorting Nexin 27 regulates basal and activity-dependent trafficking of AMPARs. Proc. Natl. Acad. Sci. USA *111*, 11840–11845.

Isaac, J.T.R., Nicoll, R.A., and Malenka, R.C. (1995). Evidence for silent synapses: implications for the expression of LTP. Neuron *15*, 427–434.

Jahn, R., and Scheller, R.H. (2006). SNAREs–engines for membrane fusion. Nat. Rev. Mol. Cell Biol. *7*, 631–643.

Jain, S., Farías, G.G., and Bonifacino, J.S. (2015). Polarized sorting of the copper transporter ATP7B in neurons mediated by recognition of a dileucine signal by AP-1. Mol. Biol. Cell *26*, 218–228.

Jullié, D., Choquet, D., and Perrais, D. (2014). Recycling endosomes undergo rapid closure of a fusion pore on exocytosis in neuronal dendrites. J. Neurosci. *34*, 11106–11118.

Jurado, S., Goswami, D., Zhang, Y., Molina, A.J.M., Südhof, T.C., and Malenka, R.C. (2013). LTP requires a unique postsynaptic SNARE fusion machinery. Neuron *77*, 542–558.

Kaech, S., and Banker, G. (2006). Culturing hippocampal neurons. Nat. Protoc. *1*, 2406–2415.

Keith, D.J., Sanderson, J.L., Gibson, E.S., Woolfrey, K.M., Robertson, H.R., Olszewski, K., Kang, R., El-Husseini, A., and Dell'acqua, M.L. (2012). Palmitoylation of A-kinase anchoring protein 79/150 regulates dendritic endosomal targeting and synaptic plasticity mechanisms. J. Neurosci. *32*, 7119–7136.

Kennedy, M.J., and Ehlers, M.D. (2006). Organelles and trafficking machinery for postsynaptic plasticity. Annu. Rev. Neurosci. *29*, 325–362.

Kennedy, M.J., and Ehlers, M.D. (2011). Mechanisms and function of dendritic exocytosis. Neuron *69*, 856–875.

Kennedy, M.J., Davison, I.G., Robinson, C.G., and Ehlers, M.D. (2010). Syntaxin-4 defines a domain for activity-dependent exocytosis in dendritic spines. Cell *141*, 524–535.

Koike, S., and Jahn, R. (2019). SNAREs define targeting specificity of trafficking vesicles by combinatorial interaction with tethering factors. Nat. Commun. *10*, 1608.

Lauffer, B.E.L., Melero, C., Temkin, P., Lei, C., Hong, W., Kortemme, T., and von Zastrow, M. (2010). SNX27 mediates PDZ-directed sorting from endosomes to the plasma membrane. J. Cell Biol. *190*, 565–574.

Laufman, O., Hong, W., and Lev, S. (2011). The COG complex interacts directly with Syntaxin 6 and positively regulates endosome-to-TGN retrograde transport. J. Cell Biol. *194*, 459–472.

Leto, D., and Saltiel, A.R. (2012). Regulation of glucose transport by insulin: traffic control of GLUT4. Nat. Rev. Mol. Cell Biol. *13*, 383–396.

Levet, F., Tønnesen, J., Nägerl, U.V., and Sibarita, J.-B. (2020). SpineJ: A software tool for quantitative analysis of nanoscale spine morphology. Methods *174*, 49–55.

Lin, D.-T., Makino, Y., Sharma, K., Hayashi, T., Neve, R., Takamiya, K., and Huganir, R.L. (2009). Regulation of AMPA receptor extrasynaptic insertion by 4.1N, phosphorylation and palmitoylation. Nat. Neurosci. *12*, 879–887.

Lin, P.-Y., Chanaday, N.L., Horvath, P.M., Ramirez, D.M.O., Monteggia, L.M., and Kavalali, E.T. (2020). VAMP4 Maintains a Ca^{2+}-Sensitive Pool of Spontaneously Recycling Synaptic Vesicles. J. Neurosci. *40*, 5389–5401.

Lledo, P.M., Zhang, X., Südhof, T.C., Malenka, R.C., and Nicoll, R.A. (1998). Postsynaptic membrane fusion and long-term potentiation. Science *279*, 399–403.

Lu, W., Man, H., Ju, W., Trimble, W.S., MacDonald, J.F., and Wang, Y.T. (2001). Activation of synaptic NMDA receptors induces membrane insertion of new AMPA receptors and LTP in cultured hippocampal neurons. Neuron *29*, 243–254.

Lüscher, C., Xia, H., Beattie, E.C., Carroll, R.C., von Zastrow, M., Malenka, R.C., and Nicoll, R.A. (1999). Role of AMPA receptor cycling in synaptic transmission and plasticity. Neuron *24*, 649–658.

Mallard, F., Tang, B.L., Galli, T., Tenza, D., Saint-Pol, A., Yue, X., Antony, C., Hong, W., Goud, B., and Johannes, L. (2002). Early/recycling endosomes-to-TGN transport involves two SNARE complexes and a Rab6 isoform. J. Cell Biol. *156*, 653–664.

Martineau, M., Somasundaram, A., Grimm, J.B., Gruber, T.D., Choquet, D., Taraska, J.W., Lavis, L.D., and Perrais, D. (2017). Semisynthetic fluorescent pH sensors for imaging exocytosis and endocytosis. Nat. Commun. *8*, 1412.

Nicholson-Fish, J.C., Kokotos, A.C., Gillingwater, T.H., Smillie, K.J., and Cousin, M.A. (2015). VAMP4 Is an Essential Cargo Molecule for Activity-Dependent Bulk Endocytosis. Neuron *88*, 973–984.

Pan, X., Zaarur, N., Singh, M., Morin, P., and Kandror, K.V. (2017). Sortilin and retromer mediate retrograde transport of Glut4 in 3T3-L1 adipocytes. Mol. Biol. Cell *28*, 1667–1675.

Park, M., Penick, E.C., Edwards, J.G., Kauer, J.A., and Ehlers, M.D. (2004). Recycling endosomes supply AMPA receptors for LTP. Science *305*, 1972–1975.

Park, M., Salgado, J.M., Ostroff, L., Helton, T.D., Robinson, C.G., Harris, K.M., and Ehlers, M.D. (2006). Plasticity-induced growth of dendritic spines by exocytic trafficking from recycling endosomes. Neuron *52*, 817–830.

Passafaro, M., Piëch, V., and Sheng, M. (2001). Subunit-specific temporal and spatial patterns of AMPA receptor exocytosis in hippocampal neurons. Nat. Neurosci. *4*, 917–926.

Peden, A.A., Park, G.Y., and Scheller, R.H. (2001). The Di-leucine motif of vesicle-associated membrane protein 4 is required for its localization and AP-1 binding. J. Biol. Chem. *276*, 49183–49187.

Penn, A.C., Zhang, C.L., Georges, F., Royer, L., Breillat, C., Hosy, E., Petersen, J.D., Humeau, Y., and Choquet, D. (2017). Hippocampal LTP and contextual learning require surface diffusion of AMPA receptors. Nature *549*, 384–388.

Proux-Gillardeaux, V., Gavard, J., Irinopoulou, T., Mège, R.-M., and Galli, T. (2005). Tetanus neurotoxin-mediated cleavage of cellubrevin impairs epithelial cell migration and integrin-dependent cell adhesion. Proc. Natl. Acad. Sci. USA *102*, 6362–6367.

Raingo, J., Khvotchev, M., Liu, P., Darios, F., Li, Y.C., Ramirez, D.M.O., Adachi, M., Lemieux, P., Toth, K., Davletov, B., and Kavalali, E.T. (2012). VAMP4 directs synaptic vesicles to a pool that selectively maintains asynchronous neurotransmission. Nat. Neurosci. *15*, 738–745.

Rimbault, C., Maruthi, K., Breillat, C., Genuer, C., Crespillo, S., Puente-Muñoz, V., Chamma, I., Gauthereau, I., Antoine, S., Thibaut, C., et al. (2019). Engineering selective competitors for the discrimination of highly conserved protein-protein interaction modules. Nat. Commun. *10*, 4521.

Roman-Vendrell, C., Chevalier, M., Acevedo-Canabal, A.M., Delgado-Peraza, F., Flores-Otero, J., and Yudowski, G.A. (2014). Imaging of kiss-and-run exocytosis of surface receptors in neuronal cultures. Front. Cell. Neurosci. *8*, 363.

Rosendale, M., Jullié, D., Choquet, D., and Perrais, D. (2017). Spatial and Temporal Regulation of Receptor Endocytosis in Neuronal Dendrites Revealed by Imaging of Single Vesicle Formation. Cell Rep. *18*, 1840–1847.

Royo, M., Gutiérrez, Y., Fernández-Monreal, M., Gutiérrez-Eisman, S., Jiménez, R., Jurado, S., and Esteban, J.A. (2019). A retention-release mechanism based on RAB11FIP2 for AMPA receptor synaptic delivery during long-term potentiation. J. Cell Sci. *132*, 132.

Sampo, B., Kaech, S., Kunz, S., and Banker, G. (2003). Two distinct mechanisms target membrane proteins to the axonal surface. Neuron *37*, 611–624.

Sankaranarayanan, S., and Ryan, T.A. (2000). Real-time measurements of vesicle-SNARE recycling in synapses of the central nervous system. Nat. Cell Biol. *2*, 197–204.

Sankaranarayanan, S., De Angelis, D., Rothman, J.E., and Ryan, T.A. (2000). The use of pHluorins for optical measurements of presynaptic activity. Biophys. J. *79*, 2199–2208.

Schoch, S., Deák, F., Königstorfer, A., Mozhayeva, M., Sara, Y., Südhof, T.C., and Kavalali, E.T. (2001). SNARE function analyzed in synaptobrevin/VAMP knockout mice. Science *294*, 1117–1122.

Sposini, S., Rosendale, M., Claverie, L., Van, T.N.N., Jullié, D., and Perrais, D. (2020). Imaging endocytic vesicle formation at high spatial and temporal resolutions with the pulsed-pH protocol. Nat. Protoc. *15*, 3088–3104.

Tanaka, H., and Hirano, T. (2012). Visualization of subunit-specific delivery of glutamate receptors to postsynaptic membrane during hippocampal long-term potentiation. Cell Rep. *1*, 291–298.

Temkin, P., Morishita, W., Goswami, D., Arendt, K., Chen, L., and Malenka, R. (2017). The Retromer Supports AMPA Receptor Trafficking During LTP. Neuron *94*, 74–82.e5.

Tran, T.H.T., Zeng, Q., and Hong, W. (2007). VAMP4 cycles from the cell surface to the trans-Golgi network via sorting and recycling endosomes. J. Cell Sci. *120*, 1028–1041.

van der Sluijs, P., and Hoogenraad, C.C. (2011). New insights in endosomal dynamics and AMPA receptor trafficking. Semin. Cell Dev. Biol. *22*, 499–505.

Vuong, C.K., Wei, W., Lee, J.-A., Lin, C.-H., Damianov, A., de la Torre-Ubieta, L., Halabi, R., Otis, K.O., Martin, K.C., O'Dell, T.J., and Black, D.L. (2018). Rbfox1 Regulates Synaptic Transmission through the Inhibitory Neuron-Specific vSNARE Vamp1. Neuron *98*, 127–141.e7.

Wang, X.B., Yang, Y., and Zhou, Q. (2007). Independent expression of synaptic and morphological plasticity associated with long-term depression. J. Neurosci. *27*, 12419–12429.

Wang, Z., Edwards, J.G., Riley, N., Provance, D.W., Jr., Karcher, R., Li, X.-D., Davison, I.G., Ikebe, M., Mercer, J.A., Kauer, J.A., and Ehlers, M.D. (2008). Myosin Vb mobilizes recycling endosomes and AMPA receptors for postsynaptic plasticity. Cell *135*, 535–548.

Welz, T., Wellbourne-Wood, J., and Kerkhoff, E. (2014). Orchestration of cell surface proteins by Rab11. Trends Cell Biol. *24*, 407–415.

Williams, D., and Pessin, J.E. (2008). Mapping of R-SNARE function at distinct intracellular GLUT4 trafficking steps in adipocytes. J. Cell Biol. *180*, 375–387.

Wu, D., Bacaj, T., Morishita, W., Goswami, D., Arendt, K.L., Xu, W., Chen, L., Malenka, R.C., and Südhof, T.C. (2017). Postsynaptic synaptotagmins mediate AMPA receptor exocytosis during LTP. Nature *544*, 316–321.

Yudowski, G.A., Puthenveedu, M.A., Leonoudakis, D., Panicker, S., Thorn, K.S., Beattie, E.C., and von Zastrow, M. (2007). Real-time imaging of discrete exocytic events mediating surface delivery of AMPA receptors. J. Neurosci. *27*, 11112–11121.

STAR★METHODS

KEY RESOURCE TABLE

REAGENT or RESOURCE	SOURCE	IDENTIFIER
Antibodies		
Rabbit anti VAMP4	Synaptic Systems	Cat# 136002, RRID AB_887816
Mouse anti Rab11	BD Biosciences	Cat# 610657, RRID AB_397984
Rabbit anti GluA1	Sigma Aldrich	Cat# AB1504, RRID AB_2113602
Mouse anti VAMP2	Synaptic Systems	Cat# 104211, RRID AB_2619758
Rabbit anti FIP2	Antibodies Online	Cat# ABIN6275434, RRID AB_11206004
Chicken anti mScarlet	Synaptic Systems	Cat# 409006, RRID AB_2725776
Mouse anti actin	Sigma Aldrich	Cat# A5316, RRID AB_476743
Chemicals, peptides, and recombinant proteins		
D-APV	Abcam	Cat# ab120003
Picrotoxin	Sigma	Cat# P1675
Strychnine hydrochloride	Sigma	Cat# S8753
Experimental models: Organisms/strains		
Rat, Sprague Dawley	Janvier Labs	N/A
Oligonucleotides		
VAMP4 shRNA1 target sequence	CTATCTTTATTTAACAACA	N/A
VAMP4 shRNA2 target sequence	GGACCATCTGGACCAAGAT	N/A
scramble shRNA	AATTCTCCGAACGTGTCAC	N/A
Recombinant DNA		
SEP-GluA1	Jullié et al., 2014; Rosendale et al., 2017	N/A
TfR-SEP	Jullié et al., 2014; Rosendale et al., 2017	N/A
VAMP4-SEP	This paper	Addgene 174406
VAMP2-SEP	Martineau et al., 2017	N/A
TeNT-LC	Proux-Gillardeaux et al., 2005	N/A
TeNT-LC E234Q	Proux-Gillardeaux et al., 2005	N/A
VAMP4-HA	This paper	N/A
Homer1c-tdTomato	Rosendale et al., 2017	N/A
VAMP2-SNAPtag	Martineau et al., 2017	N/A
VAMP4 KD1 mScarlet	This paper	Addgene 174407
VAMP4 KD2 mScarlet	This paper	Addgene 174408
Software and algorithms		
Metamorph 7.10	https://www.moleculardevices.com/products/cellular-imaging-systems/acquisition-and-analysis-software/metamorph-microscopy	N/A
MATLAB 2018b	https://fr.mathworks.com	N/A
Custom MATLAB scripts	Exo_BD_analysis	DOI 10.5281/zenodo.5146169
Igor Pro 6.0	https://www.wavemetrics.com/	N/A
imageJ 1.53c	http://www.imagej.nih.gov/ij	N/A
SpineJ 1.0	https://github.com/flevet/SpineJ	N/A

RESOURCE AVAILABILITY

Lead contact

Further information and requests for resources and reagents should be directed to and will be fulfilled by the lead contact, David Perrais (david.perrais@u-bordeaux.fr).

Materials availability

Plasmids generated in this study have been deposited to Addgene (VAMP4-SEP #174406, VAMP4 KD1 mScarlet shRNA #174407, VAMP4 KD2 mScarlet shRNA #174408).

Data and code availability

- Microscopy and electrophysiology data will be shared by the lead contact upon request.
- Most of the code used for data analysis (visualization of events, fluorescence quantification, measures of frequency) are available as a MATLAB toolbox "scission_analysis" (https://fr.mathworks.com/matlabcentral/fileexchange/72744-scission_analysis) and further described in (Sposini et al., 2020). Additional code is available in the form of a MATLAB toolbox "ExoBD_analysis" available on Zenodo (DOI 10.5281/zenodo.5146169)
- Any additional information required to reanalyze the data reported in this paper is available from the lead contact upon request.

EXPERIMENTAL MODEL AND SUBJECT DETAILS

Sprague-Dawley rats (Janvier Labs) of either sex were used at E18 for dissociated primary cultures and P6-7 for organotypic slice cultures. Timed pregnant rats were received at stage E15 and kept in the IINS animal facility until use. All the animals were used according to the guidelines of the University of Bordeaux/CNRS Animal Care and Use Committee.

METHOD DETAILS

Plasmid constructs and lentiviral vectors

VAMP4-GFP (GFP in N-terminal), VAMP7-SEP, TeNT-LC and TeNT-LC E234Q were kindly provided by Thierry Galli (IPNP, Paris, France). TfR-mCherry was kindly given by Gary Banker (OHSU, Portland, USA). VAMP2-SEP was given by Jürgen Klingauf (University of Munster, Germany) and used previously in the laboratory (Martineau et al., 2017). TfR-SEP and SEP-GluA1 were used in previous publications from the laboratory (Jullié et al., 2014; Rosendale et al., 2017). To generate VAMP4-SEP, we amplified VAMP4 from the VAMP4-GFP plasmid by PCR with the following primers: forward: GAATTCgccaccatgcctcccaagtttaagcgccacc reverse: GGATCCgaag-tacggtatttcatgac. The amplification products were sub-cloned in the TfR-SEP plasmid using BamHI and EcoRI. To downregulate VAMP4, we have tested three different sequences, with two producing large knock-down in neurons, as tested with immunofluorescence (Figure 2C). For the shRNA VAMP4 KD1 we targeted the 3′UTR. Forward: GATCCCCCTATCTT TATTTAACAACATTCAAGAGATGTTGTTAAATAAAGATAGTTTTTC Reverse: TCGAGAAAAACTATCTTTATTTAACAACATCTCTT GAATGTTGTTAAATAAAGATAGGGG. The sequence for the shRNA VAMP4 KD2 is almost identical to a published siRNA designed to knock-down VAMP4 in human cells (Gordon et al., 2010), shifted by one nucleotide. The rat and human sequences are identical in this part of the VAMP4 gene. Forward: GATCCCCGGACCATCTGGACCAAGATTTCAAGAGAATCTTGGTCCAGATGGTCCTTTTTC. Reverse: TCGAGAAAAAGGACCATCTGGACCAAGATTCTCTTGAAATCTTGGTCCAGATGGTCCGGG. These two strands were inserted in the pSuper neo GFP vector (Oligoengine) after hybridation, using BglII and XhoI restriction sites. Scramble shRNA is provided by Oligoengine. To generate VAMP4-HA for rescue experiments, we amplified the tenth subunit of the human fibronectin type III fused with hemagglutinin tag (HA) from a plasmid as in (Rimbault et al., 2019) with the following primers: Forward: GTCGGATC CACCGGTCGGTAGTTCTCCGCGTGGTTCG. Reverse: GTCGCTAGCTCAGCCCACGCGTGGTGCATAGTC and inserted in the VAMP-SEP plasmid with BamHI and NheI. Lentiviral vectors were constructed from the FHUG+W lentiviral vector (Addgene #74011, kind gift from Oliver Schlüter, University of Pittsburgh, USA). GFP was substituted with mScarlet, a bright monomeric red fluorescent protein (Bindels et al., 2017) with a synthetic gene (Eurofins) and appropriate restriction sites for AgeI and XbaI. The shRNAs scr, KD1 and KD2 were inserted from the corresponding shRNA vectors with EcoRI and XhoI. Lentiviral vectors were made by the service platform for lentiviral vector production "Vect'UB' of the TMB-Core of the Bordeaux University. They were produced by transient transfection of 293T cells according to standard protocols. Viral titers were estimated by comparing p24 antigen levels of each lentiviral supernatant measured in the concentrated viral supernatants by an enzyme-linked immunosorbent assay (Innotest HIVp24; INGEN,Rungis, France) with a similar EGFP lentiviral supernatant produced simultaneously.

Primary neuronal cultures and transfection

Dissociated hippocampal neurons from E18 Sprague-Dawley rat embryos of either sex were prepared as described (Kaech and Banker, 2006). All the animals were used according to the guidelines of the University of Bordeaux/CNRS Animal Care and Use

Committee. Cells were plated at a density of 2-4 10^5 cells per 60-mm dish on poly-L-lysine pre-coated coverslips and put after 4 h in the 'sandwich configuration' in dishes containing confluent astrocytes. Cultures were maintained at 36.5°C, 5% CO_2 in Neurobasal medium (Thermofisher Scientific cat # 21103049) supplemented with 2 mM L-glutamine and B27 plus (Thermofisher Scientific cat # A3582801) or SM1 (Stemcell technologies cat # 05711) neuronal supplement, during at least 6 days. After 6 days, media was supplemented with cytosine arabinoside (5 μM) to inhibit glial cell proliferation. The cultures were either (i) left in this medium, renewed by a third twice a week or (ii) replaced by a third twice a week with BrainPhys medium (StemCell Technologies, cat # 05791) supplemented with SM1 neuronal supplement. Experiments in Figures 1 and 2 were performed with cultures prepared with protocol (i). When we tried to evoke cLTP with this type of culture, we got very inconsistent results, even though we tried to vary many parameters such as cell density, age of culture (up to 20 DIV), temperature, glucose concentration, pre-incubation for up to 1 h in imaging medium. Therefore, for all cLTP experiments (Figures 3, 4, and 5), we used cultures prepared with protocol (ii), which gave much more robust results. We interpret this difference with the documented increase in electrical activity in cultures using BrainPhys (Bardy et al., 2015).

Neurons were transfected at 7-14 DIV with the different cDNA with Effectene (QIAGEN, cat # 301425) following manufacturer's protocol with 1-3 μg of DNA per dish containing 4 coverslips, or with the calcium phosphate procedure (6 μg / dish). Experiments were performed 1 to 7 days after transfection (12-17 days *in vitro*), depending on the degree of neuronal maturation required. Lentivirus VAMP4 KD or scr vectors were applied after 4 DIV with twice as many particles as neurons.

Organotypic hippocampal slice preparation and transfection

All animal experiments complied with all relevant ethical regulations (study protocol approved by the Ethical Committee of Bordeaux CE50). Animals were raised in our animal facility; they were handled and euthanized according to European ethical rules. Hippocampi were dissected from wild-type rats at postnatal age 7-8 in ice-cold low sodium dissection solution containing (in mM): 1 $CaCl_2$, 10 D-glucose, 4 KCl, 5 $MgCl_2$, 26 $NaHCO_3$, 234 sucrose, 0.1% v/v phenol red solution 0.5% in DPBS. Transverse slices (350 μm) were cut with a tissue chopper (McIlwain) and positioned on small membrane segments (FHLC01300, Millipore) and culture inserts (PICM0RG50, Millipore) in 6-well plates containing 1 ml/well slice culture medium. Culture medium was composed of minimum essential medium (MEM) supplemented with 15% heat-inactivated horse serum, 0.25 mM ascorbic acid, 1 mM L-glutamine, 1 mM $CaCl_2$, 2 mM $MgSO_4$, 30 mM HEPES, 5.2 mM $NaHCO_3$, 13 mM D-glucose and 1 mg/L insulin (pH 7.3, osmolarity adjusted to 320). Slices were maintained in an incubator at 35°C with 5% CO2 and the culture medium was replaced every 2-3 days.

Transduction of neurons with lentiviral vectors (scr/KD1/KD2 mScarlet) was done 24 h after slice preparation. A pulled glass pipette (4-5 Mohm) was loaded with virus (10^6-10^7 particles per μl) and then lowered into the CA1 region of the slice. A Picospritzer (Parker Hannifin, NJ, USA) was used to pulse the virus into the slice. Single cell electroporation (with TeNT-LC or TeNT-LC E234Q and GFP) was performed at 3-4 DIV. Slices were individually transferred to the chamber of an upright microscope (Eclipse FN1, Nikon). The microscope chamber was cleaned with 70% ethanol before the beginning of the experiment. The chamber contained sterile-filtered bicarbonate-containing Tyrode's solution maintained at ambient temperature and atmospheric conditions without perfusion. Bicarbonate-containing Tyrode's solution was composed of (in mM): 120 NaCl, 3.5 KCl, 2 CaCl2, 2 MgCl2, 10 HEPES, 10 D-Glucose, 2 NaHCO3 and 1 Na-pyruvate (pH 7.3, 300 mOsm). Patch pipettes (~5 Mohm) pulled from 1.5 mm borosilicate capillaries (Harvard Apparatus) were filled with potassium-based solution composed of (in mM): 135 K-methanesulfonate, 4 NaCl, 10 HEPES, 0.06 EGTA, 0.01 $CaCl_2$, 2 $MgCl_2$, 2 Na2-ATP and 0.3 Na-GTP (pH 7.3, 280 mOsm) supplemented with plasmid DNA (13 ng/μL). After obtaining a loose patch seal, electroporation was performed by applying 4 square pulses of negative voltage (−2.5 V, 25 ms duration) at 1 Hz, then the pipette was gently retracted. A total of 10–20 neurons were electroporated per slice, and the slice was placed back in the incubator for 3-4 days before electrophysiology recordings.

Live cell imaging of cultured neurons

Fluorescent cells were imaged with a spinning disk confocal microscope which consisted in a Leica DMI6000 inverted microscope (Leica Microsystems, Wetzlar, Germany) equipped with a Confocal Scanner Unit CSU22 (Yokogawa Electric Corporation, Tokyo, Japan), an HCX Plan Apo 63x oil objective (NA 1.4) (for exocytosis events) or Plan Apo 40x oil immersion objective (for estimation of surface fluorescence or FRAP) and a QuantEM or an Evolve camera (Molecular Devices). Illumination was achieved by a 473 nm laser, and for 2 color imaging, by alternating 473 and 532 nm lasers. The whole system was controlled by MetaMorph 7.8 software (Roper Scientific, France). Transfected neurons were mounted in imaging chamber perfused with HEPES buffered solution (HBS) with the following (in mM): 120 NaCl, 5 KCl, 2 MgCl2, 2 CaCl2, 25 HEPES, and 25 D-glucose, adjusted to pH 7.4. Imaging was done at 37°C.

To detect exocytosis events, we performed time lapse 1- or 2-color imaging at 1 Hz for 2-5 min. For the ppH protocol, we used as described previously (Jullié et al., 2014) an Olympus IX71 inverted epifluorescence microscope equipped with a Zeiss Plan Fluar 100x oil objective (NA 1.45). Epifluorescence illumination was done with 470 nm LED (Rapp Opto-electronics, Germany) and an ET525/50 m emission filter (Chroma Technologies). The camera was controlled by MetaVue (Molecular Devices) and the electrovalves were controlled by a patch clamp amplifier (HEKA). Cells were alternatively perfused with HBS and MBS every 2 s. MBS has the composition as HBS except that HEPES is replaced with MES and the pH is adjusted to 5.5. To estimate surface expression levels of TfR and GluA1, cells were imaged with the spinning disk confocal. z stacks were taken, first perfused with HBS then with MBS

(pH 5.5), then back to HBS (pH 7.4). Finally, the cells were perfused in HBS where 50 mM NaCl is substituted for 50 mM NH_4Cl (pH 7.4, HBS NH4 solution).

For cLTP experiments, we selected 2-5 transfected neurons and recorded their coordinates in a motorized microscope stage. The cLTP stimulation solution contained (in mM): 125 NaCl, 2 $CaCl_2$, 5 KCl, 25 HEPES, 25 D-glucose, supplemented with 0.5 glycine, 0.01 strychnine, and 0.03 picrotoxin (pH 7.4). For cLTP induction, neurons were incubated in cLTP stimulation solution without glycine for 10 min, and then stimulated with glycine for 3-4 min before they were returned back to a solution containing no glycine and 2 mM $MgCl_2$. In experiments of cLTP blockade, the NMDA receptor antagonist APV (100 μM) was added to the same solutions before, during and after cLTP induction. Picrotoxin blocks $GABA_A$ receptors and strychnine blocks glycine receptors. It was added to avoid the potential activation of glycine receptors. For experiments on exocytosis events, we recorded before, during and after cLTP time lapse movies of cells lasting 2 min. For experiments on fluorescence recovery after photobleaching, we took a stack of 9 planes, 1 μm apart of each selected transfected neuron. Cells were photo bleached entirely using high laser power and another Z stack was taken to ensure that more than 90% reduction of fluorescence of SEP-GluA1 was achieved. Glycine (500 μM) was then perfused into the chamber for 4-5 min to induce cLTP followed by Mg2+ containing tyrode's solution for the following 20 min. The recovery of fluorescence was captured at 5 min intervals for 20 min with a series of Z stack images, which reflects SEP-GluA1 delivery to the plasma membrane.

Quantification of live cell imaging data

Detection and quantification of exocytosis was performed as described previously (Jullié et al., 2014) with macros programmed in MATLAB 2018. To highlight fast fluorescence increases reporting exocytosis events, we first constructed a differential movie (imagen+1-imagen + constant). A manual threshold was used to select candidate events (objects bigger than 2 pixels), with additional criteria to exclude moving clusters, variations in intense clusters, or tubule contraction. This threshold was calculated above the mean fluorescence of the cell mask. For each candidate event a mini-movie and a series of background-subtracted images were generated. A second screen based on this quantification discarded more events such that more than 80% were subsequently validated. Events were validated or discarded by the user based on these two visualization tools. For experiments with fast pH changes, events were detected directly on the full movie. Event frequencies were normalized by the surface of the cell mask.

For fluorescence quantification, performed as in Jullié et al. (2014), a region of interest (ROI) and a region surrounding the ROI (SR) are defined as follows. The five background subtracted images before exocytosis define a standard deviation (SD) of pixel values. A threshold is defined as 7 times the SD to define putative ROIs. In case of multiple objects, the one closest to image center is chosen. If no object is detected, the ROI is defined as a 2.2 pixel (380 nm) radius circle centered on the centroid of the original detection. If an object is detected, the ROI is the reunion of the object and a 2.2 pixel radius circle centered on the object. The SR is obtained by a dilation of the ROI by 2 pixels. For the following frame, the same object detection procedure is applied, and a new ROI and SR are defined. The centroid of the new ROI must be less than 5 pixels away. If no object is defined, the ROI is kept the same. For images prior to exocytosis, the ROI used is the one defined at time 0, the time of exocytosis. For each event, we compute $F_{R\text{-}S} = F_{ROI} - F_{SR}$, where F_{ROI} and F_{SR} represent the average fluorescence of the original images in the ROI and the SR, respectively. For the SR the 20% lowest and highest pixel values are removed to limit environmental variations (out of the cell, bright cluster). For each event, $F_{R\text{-}S}$ is normalized by subtracting the average of values before exocytosis and divided by FR-S at the time of exocytosis. Events for which normalized FR-S was above 50% for less than two seconds were sorted as burst events and the other ones sorted as display events. For two-color experiments, red $F_{R\text{-}S}$ is quantified with the same ROI and SR defined with the SEP signal. The fluorescence is normalized by the average red fluorescence in the cell in order to limit variations between cells due to differences in expression levels. To estimate the level of enrichment of red fluorescent markers, we co-transfected neurons with TfR-SEP and mCherry, a cytosolic protein. With our quantification and normalization method, we detect no variation of mCherry fluorescence after exocytosis, and a level of average normalized fluorescence of ~1.20 for display and 1.26 for burst exocytosis (see Jullié et al., 2014). Therefore, we took as significant enrichment average measures over 1.3.

For quantification of surface fraction (Figures 2G and 5E), we selected ROIs in dendrites and spines (visible puncta during NH_4Cl perfusion), and surface expression was calculated as percentage of total $(F_{7.4} - F_{5.5}) / (F_{NH4} - F_{5.5})$.

For quantification of whole cell FRAP (Figures 5A–5D), we used maximum intensity projections of z stacks. A mask of a 50 μm-long dendritic segment was created using the first image (pre-bleach) of the time series and then applied on all images to extract total intensity under the same mask. Each intensity value was then normalized to the bleached image to calculate the SEP-GluA1 recovery percentage.

Immunocytochemistry and transferrin recycling assay

For immunocytochemistry, cells were fixed for 10 min in warm 4% paraformaldehyde-4% sucrose in phosphate buffered saline solution. After rinse with PBS, cells were permeabilized with 0.1% Triton X-100 in PBS containing 1% gelatin (to block unspecific binding) for 20 min. VAMP4 was labeled with 1/500 rabbit anti VAMP4 (Synaptic Systems 136 002, dilution 1:500), followed by Alexa Fluor 568-conjugated goat anti-rabbit antibody (Thermo Fisher Scientific A11011, dilution 1:1000). Coverslips were then mounted in Fluoromount-G (SouthernBiotech). Neurons were imaged on a Leica SP8 confocal microscope available at the Bordeaux Imaging Center, or stacks of 10 planes, 0.2 μm apart for maximum intensity projections (for quantification of KD efficiency, Figures 2C and S3). Colocalization between markers was quantified with the Coloc2 plugin of imageJ to calculate Pearson's r coefficient on selecting

portions of dendrites as ROIs with automatic threshold determination (Costes et al., 2004). For each ROI, we performed 20 randomizations to calculate corresponding r coefficients which were systematically below the actual measure, confirming the specific colocalization.

For pulse chase of transferrin, cells were starved for 5 min in HBS at 37°C 5% CO_2 before uptake of Alexa568-Tfn (ThermoFischer T23365) at 50 μg/ml for five minutes at 37°C 5% CO_2. Chase was done with unlabeled holo-Tfn (Sigma, T4132) at 2 mg/ml for 5, 10, 15 and 20 min at 37°C 5% CO_2. Cells were then fixed for 10 min in 4% paraformaldehyde-4% sucrose in PBS. Cells were imaged in PBS on the spinning disk confocal microscope. A stack of 9 focal planes, 0.2 μm apart, was acquired in both GFP and A568-Tfn channel. We defined a mask of the cell in the GFP channel and used it for quantification of A568-Tfn labeling.

Electron microscopy

Coverslips with attached neurons were placed in pre-warmed 4% paraformaldehyde (EMS 15710) in 0.15M Sorensen's phosphate buffer (PB, EMS 11682) at room temperature for 45 minutes. All subsequent steps were performed at room temperature. Neurons were rinsed 3 times in 0.15 M Sorensen's PB, once in 0.1M Millonig's PBS, and then blocked and permeabilized in a solution containing 0.1M Millonig's PBS with 2% BSA (Sigma 3359), 0.1% cold water fish skin gelatin (Aurion 900.033) and 0.1% Saponin for 60 minutes. Next, neurons were incubated for 90 minutes in primary antibody against TfR (Millipore) or VAMP4 (Synaptic System) diluted in the blocking/Saponin solution. Then, coverslips were rinsed twice in blocking/Saponin solution for 60 minutes before incubation with FluoroNanogold anti mouse Fab' Alexa Fluor 488 for TfR or anti rabbit Fab' Alexa Fluor 488 for VAMP4 (Nanoprobes ref# 7202) diluted 1:100 in blocking/Saponin solution for 60 minutes, then rinsed once in Sorensen's PB, and placed in freshly prepared 2% paraformaldehyde in Sorensen's PB for 30 minutes to stabilize immunogold labeling. After, neurons were stored in Sorensen's PB until silver intensification. In some cases, the quality of FluorNanogold labeling was confirmed by epifluorescence microscopy (Leica DM5000) before proceeding with electron microscopy.

FluoroNanogold was enhanced for 5-7 minutes using HQ Silver Reagent (Nanoprobes ref# 2012) according to manufacturer's instructions and processed immediately for electron microscopy; all steps were carried out at room temperature. After several rinses in Sorensen's PB, neurons were incubated in 0.2% OsO_4 in Sorensen's PB for 30 minutes, and then rinsed 10 times in dH_2O to remove all traces of PB before placing neurons in filtered 0.25% uranyl acetate dissolved in dH_2O for 30 minutes. After several water rinses, neurons were dehydrated by 3 minute incubations in a graded series of ethanol: 50%, 70%, 95%, and twice in 100%. No propylene oxide was used to prevent loss of immunogold label. Samples were infiltrated during 1-2 hour steps in 70% Epon812/ ethanol mixture followed by 2 exchanges of 100% freshly prepared Epon812 (Taab, T004), and finally embedded in freshly prepared Epon812. To allow cutting of *en face* sections of neurons, coverslips were placed cell side facing up on a glass slide and gelatin capsules filled with Epon812 were inverted and placed on top of coverslip, and polymerized at 60°C for 48 hours. Coverslips were removed from polymerized samples by gentle heating over a flame while pulling slightly on the glass slide. Ultrathin sections (60 nm thickness) were cut using an Ultra 35° diamond knife (Diatome, USA) and a Leica Ultracut UCT M26 (Leica Microsystems, Germany) and picked up on 2mm slot grids with a 1% formvar support film. Sections were contrasted with 3% aqueous uranyl acetate for 5 minutes, and then Reynolds's lead citrate for 5 minutes prior to imaging using a Hitachi H7650 transmission electron microscope operated at 80kV. Images were captured using an Orius CCD (Gatan Soc., USA).

Membrane fractionation in sucrose gradient

Synaptosomal fractionation was carried out as previously described (De-Smedt-Peyrusse et al., 2018), and microsomal fractionation was adapted from another study (Royo et al., 2019). Briefly, 2 rat hippocampi (approximatively 130 mg) were mechanically homogenized in an isotonic buffer containing 10.9% sucrose, 4mM HEPES (pH 7.4), and a cocktail of protease inhibitors from Calbiochem (Protease Inhibitor Cocktail Set III, EDTA-Free). The homogenate was centrifuged at 1000 g for 5 min at 4°C. The first supernatant (S1) was centrifuged at 12,500 g for 8 min at 4°C. 700 μL of the second supernatant (S2, microsomal fraction), containing 10.9% sucrose, was loaded on top of a discontinuous sucrose gradient, in 4 mM HEPES (pH 7.4), containing layers of 15%, 20%, 25%, 30%, 35%, 40% and 45% sucrose (from top to bottom), each layer with a volume of 200 μl. Lastly, a floating layer of 5% sucrose (100 μL) was loaded on top of the S2. The gradient was centrifuged at 62,000 g for 4 h 20 min at 4°C using an Optima Max XP ultracentrifuge with a TLS-55 swing rotor (Beckman Coulter). Fractions of 100 μl were collected from top to bottom and analyzed by capillary electrophoresis based immunoblot (WES from proteinsimple, California, USA) with antibodies specific to GluA1, Rab11, FIP2, VAMP2, and VAMP4 and secondary antibodies as described below.

WES (Simple Western) immunodetection of the membrane fractionation

Detection proteins of interest were determined using WES (Simple Western) by Protein Simple©. The Simple Western system uses automated capillary electrophoresis to separate, identify and quantify a protein of interest. Reagents (Dithiothreitol, DTT; Fluorescent 5X Master Mix, Biotinylated Ladder) were prepared according to the manufacturer protocol. Samples were diluted with 0.1X Sample Buffer (after dilution of 10X Sample Buffer 1:100 with water), combined with 5X Master Mix (1 MasterMix:4 Sample) to obtain 200 ng/mL (for Rab11 and VAMP4) or 50 ng/mL (for GLUA1, VAMP2 and FIP2) and finally denatured 5 min at 70°C. Antibodies were diluted to their optimal concentration (Rab11 1:50, BD Bioscience #610657; VAMP4 1:50, Synaptic Systems #136002; GLUA1 1:50, Sigma Aldrich #AB1504; VAMP2 1:50, Synaptic Systems #104211; FIP2 1:250, antibodies-online #ABIN6275434) and Luminol (200 μL)-Peroxide (200 μL) mix was prepared. A 12-230 or 2-40 kDa Simple Western plate was finally filled following

the manufacturer protocol scheme: (5 μL of Biotinylated Ladder, 4 μL of Samples, 10 μL of Wes Antibody Diluent II, 10 μL of Primary Antibody, 10 μL of Streptavidin-HRP, 10 μL of Secondary Antibody and 15 μL of Luminol-Peroxide Mix). Simple Western standard immunodetection protocol was run. The system captured data as a chemiluminescent image of the capillary through a charge-coupled device (CCD) camera. Capillary images were analyzed by the manufacturer Compass software. Briefly, the protein peaks area under the curve (AUC) were fitted using a Gaussian distribution. The Gaussian fitted protein AUC was expressed as a ratio to the average of all the Gaussian fitted protein AUC fractions.

Whole-cell patch clamp recordings

Organotypic slices (8-10 days in culture) were transferred to an upright Leica DM5000 microscope (Leica Microsystems, Wetzlar, Germany) chamber perfused with carbogen-bubbled recording ACSF maintained at ~30°C by an in-line solution heater (WPI). For whole-cell voltage clamp recordings of evoked EPSCs amplitudes, the recording ACSF contained (in mM): 125 NaCl, 26 $NaHCO_3$, 10 D-glucose, 1.26 NaH_2PO_4, 3 KCl, 2 $CaCl_2$, 1 $MgCl_2$, 0.025 picrotoxin (320 mOsm). Patch pipettes (~4-6 Mohm) for whole-cell voltage clamp recordings were filled with a caesium-based intracellular solution containing (in mM): 130 Cs-methanesulfonate, 4 NaCl, 10 HEPES, 5 QX-314 Cl, 1 EGTA, 2 Mg-ATP, 0.5 Na-GTP, 10 phosphocreatine (pH 7.3, 290 mOsm). To evoke an EPSC, Schaffer collaterals were activated at 0.1 Hz using a Platinum-Iridium cluster bipolar stimulating electrode (25 μm, FHC, USA) positioned in stratum radiatum of CA1 region. AMPAR-mediated currents were recorded by clamping the neuron at −70 mV and NMDAR-mediated currents were recorded at +40 mV and measured 100 ms after the stimulus.

Dual cell recordings of neighboring transfected/transduced and intact pairs of pyramidal cells were recorded simultaneously in CA1 with Schaffer collateral stimulation. The AMPAR/NMDAR ratio was calculated as the peak averaged AMPAR EPSCs (30 consecutive events) divided by the averaged NMDAR EPSCs (30 consecutive events). Stimulation control, analog signal filtering and digitization were performed with EPC-10 USB amplifier controlled by Patchmaster Next software (HEKA Elektronik).

For LTP recordings, the CA3 region was cut off, and slices were continuously perfused with warm (30°C), carbogen (95% O2 / 5% CO2)-bubbled recording ACSF containing in (mM): 125 NaCl, 26 $NaHCO_3$, 10 D-glucose, 1.26 NaH_2PO_4, 3 KCl, 4 $CaCl_2$, 4 $MgCl_2$, 0.025 picrotoxin. Calcium and magnesium concentrations were raised to 4mM to dampen excitability. Strictly 5 min after going whole-cell, LTP was induced by depolarization of the cells to 0 mV while stimulating the afferent Schaffer's collaterals at 3 Hz for 100 s. Pre-stimulation baseline was recorded for 3 min at 0.1 Hz. Short baseline recordings were necessary to prevent washout of LTP in slice culture whole-cell recordings.

Quantification of spine morphology

Neurons in organotypic slices were transfected with mScarlet-KD or scramble shRNA constructs by single-cell electroporation. 4 days later, slices were fixed with 4% paraformaldehyde- 4% sucrose in PBS for 4 h and processed for imaging with a Leica DMI6000 TCS SP5 microscope using a 63 × /1.4 NA oil objective. Z-tacks of 29 images (200 nm apart, 80 nm pixel size were acquired at a scanning frequency of 400 Hz and maximum intensity projections computed. Spines were detected and measured with the imageJ plugin SpineJ (Levet et al., 2020).

QUANTIFICATION AND STATISTICAL ANALYSIS

All data is presented as mean ± SEM. Statistical significance was calculated on Graphpad Prism 8 software. We used two-tailed t test between interleaved control cells and test cells or one-way ANOVA followed by Dunnett's test for multiple comparisons. Significance was depicted in Figures by the following symbols: * ($p < 0.05$) ** ($p < 0.01$) *** ($p < 0.001$) and exact p values are presented in the text or Figure legends when applicable.